doi.org/10.1111/jmi.12895

Fluorescence visualization of cellulose and pectin in the primary plant cell wall

Amir J. Bidhendi, Youssef Chebli, Anja Geitmann*

Department of Plant Science, McGill University, Macdonald Campus, 21111 Lakeshore, Ste-Anne-de-Bellevue, Québec H9X 3V9, Canada

*Correspondence to: Anja Geitmann, Faculty of Agricultural and Environmental Sciences, McGill University, Macdonald Campus, 21111 Lakeshore, Ste-Anne-de-Bellevue, Québec H9X 3V9, Canada Tel: + 1 (514) 398 7707; e-mail: geitmann.aes@mcgill.ca

Summary

Plant cell walls constitute the extracellular matrix surrounding plant cells and are composed mainly of polysaccharides. The chemical makeup of the primary plant cell wall, and specifically, the abundance, localization, and arrangement of the constituting polysaccharides are intimately linked with growth, morphogenesis, and differentiation in plant cells. Visualization of the cell wall components is, therefore, a crucial tool in plant cell developmental studies. In this technical update, we present protocols for fluorescence visualization of cellulose and pectin in selected plant tissues and illustrate examples of some of the available labels that hold promise for live imaging of plant cell wall expansion and morphogenesis.

Keywords

Cell development, cellulose, confocal laser scanning microscopy, fluorescence microscopy, immunohistochemistry, label, live cell imaging, pectin, polysaccharides, primary plant cell wall, stain.

Introduction

The primary plant cell wall is a polysaccharidic shell that encapsulates plant cells. This composite material defines cell shape and enables the establishment of turgor by resisting expansion due to osmotically-driven water uptake. Plant development relies on cell division, differentiation and growth. These processes involve coordinated synthesis, assembly and *in muro* modification of the cell wall constituents leading to controlled expansion of the primary cell wall. The material properties of the cell wall are a controlling parameter during cell differentiation and are tightly linked with cellular morphodynamics (Bidhendi et al., 2019, Fayant et al., 2010, Yanagisawa et al., 2015, Bidhendi & Geitmann, 2018, Rui et al., 2018, Carter et al., 2017, Bidhendi & Geitmann, 2019a, Bidhendi & Geitmann, 2019b). The mechanical properties of the cell wall are modulated by spatial distribution of the building components, their interactions, and the activities of various enzymes modifying their chemical configurations and intermolecular linkages (Altartouri & Geitmann, 2015, Echevin et al., 2019, Cosgrove, 2015, Bidhendi & Geitmann, 2016, Baskin, 2005, Somerville et al., 2004, Zhang et al., 2019). Therefore, studying the

development of plant tissues and the differentiation of plant cells inevitably involves scrutiny of spatiotemporal modifications of the cell wall composition. Despite the importance of the dynamic properties of the cell wall for various plant biological investigations ranging from fundamental plant development research to agronomy and biomimetics, the exact molecular architecture of the primary plant cell wall and the physiological implications of its modifications remain poorly understood.

The plant cell wall is located directly outside of the plasma membrane and consists primarily of a network of cellulose microfibrils, hemicelluloses, pectins, structural proteins and glycoproteins that are either delivered to or synthesized directly at the surface of the plasma membrane. Cellulose microfibrils are generally recognized as the main load-bearing polymers of the primary plant cell wall. Organized and well-aligned cellulose microfibrils, that can congregate into "superbundles" of up to several hundreds of nanometers, are thought to restrict expansion of the cell wall along their predominant orientation, creating the conditions required for anisotropic growth (Geitmann, 2010b, Bidhendi & Geitmann, 2016, Aouar et al., 2010, Burgert & Fratzl, 2009). Cellulose in the primary plant cell wall comprises crystalline and non-crystalline domains (Cosgrove, 2014) and their relative abundance affects the mechanical properties of cellulose microfibrils and the efficacy of the hydrolysing enzymes (Hall et al., 2010, Novy et al., 2019, Rongpipi et al., 2019, Cosgrove, 2018). Alteration in crystallinity or volume fraction of cellulose has been linked with abnormal shape phenotypes in growing cells (Bidhendi et al., 2019, Fujita et al., 2013, Burn et al., 2002). Pectins constitute another important class of cell wall polysaccharides. The role of pectins in modifying cell wall mechanics and driving cell morphogenesis is only emerging (Bidhendi et al., 2019, Fayant et al., 2010, Carter et al., 2017, Amsbury et al., 2016, Zhang et al., 2019, Cosgrove, 2014, Levesque-Tremblay et al., 2015, Kaplan et al., 2019). Therefore, localization and dynamics of cell wall components are essential elements required to understand the time evolution of cell wall properties and cell development.

Fluorescence microscopy is an invaluable tool in developmental biology that, by enabling real-time visualization and quantification of cellular processes, facilitates testing developmental paradigms (Mavrakis et al., 2010, Specht et al., 2017, Roca-Cusachs et al., 2017, Sahl et al., 2017, Follain et al., 2017, Schermelleh et al., 2019). Localizing cell wall components using fluorescent molecules with specific binding affinity for different cell wall polysaccharides has led to a crescendo of plant cell developmental data. Developmental research that inherently benefits from time-course imaging of a given specimen requires these molecules to operate in the living cells, and to not interfere with the normal functioning of intracellular processes during the period of experimentation. While this can be the case for some stains (e.g., propidium iodide (PI), FM dyes, fura-dextran), other stains or labels require prior fixation (e.g., antibodies, DAPI) thus precluding the observation of consecutive developmental time points. An additional complicating step of antibody labeling is that usually the target-specific antibody is not fluorescently labeled and instead, a fluorescently-tagged secondary antibody is used to locate the first antibody and, thus indirectly, the antigen. An additional limiting factor of antibodies is their considerable size which limits their ability to penetrate deeper into cells or tissues necessitating permeabilization and/or thin sectioning. Over the

Final version published in *Journal of Microscopy* doi.org/10.1111/jmi.12895

past decades, a panoply of polysaccharide-specific antibodies has been developed (Verhertbruggen et al., 2009, Knox, 1992, Liners et al., 1989, Blake et al., 2006, Hervé et al., 2011, Ruprecht et al., 2017, Knox et al., 1990, Liners & Van Cutsem, 1992, Puhlmann et al., 1994, Marcus et al., 2010, McCartney et al., 2005, Cornuault et al., 2015, Pattathil et al., 2010, Willats et al., 2000), whereas the toolbox of fluorescent probes for direct labeling is growing only slowly (Paës, 2014, Zhao et al., 2019, Anderson & Wallace, 2012, Mravec et al., 2017, Rydahl et al., 2018, Moreno et al., 2006, Wallace & Anderson, 2012, Voiniciuc et al., 2018, Samaj et al., 2017, Mravec et al., 2014) and the quest for probes with the highest specificity that also allow live-cell imaging is ongoing. The specificity of stains is often either not high or not well defined and the staining results for each dye greatly depend on the tissue type, local pH, the accessibility of binding sites and the ionic state of the cell compartment.

Regardless of the type of the cell wall probe, studying the localization of cell wall polysaccharides requires determining a working protocol that yields a satisfactory fluorescent signal from the target compartment and appropriate interpretation of the results. Here, we provide functional labeling protocols for some of the major fluorescent probes for cellulose and homogalacturonan (HG) pectin in the primary cell wall. To demonstrate general suitability, we used multiple types of plant tissues and cells: pollen tubes, epidermal pavement cells, guard cells, hypocotyl and root epidermal cells and root hairs. Each of these cell types has been used to substantially advance our understanding of plant development. Pollen tubes and root hairs grow in rod-shaped geometries, exhibiting subcellular regions with differential growth rates which facilitates the correlation between observed cell wall composition, mechanics and the resulting rod shape (Park et al., 2011, Fayant et al., 2010). Epidermal cells in the elongation zone of a root are approximately brick shaped. They are devoid of a cuticle and, therefore, absorb dyes or labels easily facilitating time-lapse visualization of cellulose reorganization (Anderson et al., 2010). Epidermal cells of leaves and cotyledons are typically more difficult to stain since they are covered by a hydrophobic cuticle. The different cell types in the leaf and cotyledon epidermis of dicotyledon plants demonstrate highly complex shapes. Pavement cells form interlocking jigsaw puzzle shapes the emergence of which was shown to correlate with a subcellularly varying distribution of cellulose and pectin (Bidhendi et al., 2019, Panteris & Galatis, 2005). The kidney-shaped profile of guard cells is related to their morphogenesis and function—the turgor-driven deformation that reversibly opens the stomatal pores controlling gas exchange (Lundgren & Fleming, 2019, Cooke et al., 1976, Yi et al., 2018, Rui et al., 2019, Bidhendi & Geitmann, 2018). In all cell types featured in this paper, the correlation between morphogenesis, form and function can be understood only through the investigation of the architectural details of their respective cell walls. In this technical update, we provide simple staining and labeling protocols for this purpose.

For pollen tubes, we demonstrate use of a series of cell wall-specific antibodies and Carbohydrate Binding Module 3a (CBM3a) in immunofluorescent labeling of cellulose and HG pectin. Using the other cell types, we also demonstrate use of a number of widely used molecular probes and a chitosan oligosaccharide-(COS) based probe. Calcofluor white (CFW, also known as fluorescent brightener 28) is a fluorescent probe that binds β-glucans, including cellulose, xyloglucans, callose, and chitin (Herth

Final version published in *Journal of Microscopy* doi.org/10.1111/jmi.12895

& Schnepf, 1980, Maeda & Ishida, 1967, Hughes & McCully, 1975). Despite its binding promiscuity (Anderson et al., 2010), CFW continues to be widely used as a fluorescent probe for visualization of plant cell walls in general, and for studying the orientation of cellulosic structures in particular (Bidhendi et al., 2019, Flores-Félix et al., 2015, Herth & Schnepf, 1980, Aouar et al., 2010, Inada et al., 2000, Anderson et al., 2010). The rationale is that in the primary plant cell wall no other cell wall polysaccharide is expected to form fibrillar structures at the scale of cellulose microfibril aggregates. Thus, interpreting the cellulose microfibril orientation in a particular tissue context is thought to be less ambiguous than the actual binding specificity of the dye. Pontamine Fast Scarlet 4B (PFS, also known as Direct Red) was originally used as a dye in the paper and textile industry (Cook, 1940, Bedrick, 1968) and is proposed to bind more specifically to cellulose. It was therefore adopted rapidly for the visualization of cellulose in plant cells (Liesche et al., 2013, Anderson et al., 2010). The COS probe tagged with Alexa Fluor 488 (hence COS^{488}) is used here to label pavement cells and pollen tubes. COS^{488} is suggested to bind the oligogalacturonate fragments of the HG, mediated through the positive charge of the amino groups on the former and the negative charge of the carboxyl group of the latter. Therefore, COS^{488} was developed to label de-esterified HG pectin (Mravec et al., 2014) and is suggested to have a number of superior characteristics compared to antibodies including faster and better penetration, and higher sensitivity to changes in degree of esterification making it potentially suitable for real-time imaging. Lastly, PI, a general cell wall stain, is used for labeling cotyledon pavement cells as well as living pollen tubes.

Materials

Plant material

Seedlings of *Arabidopsis thaliana* ecotype Col-0 were used for visualization of the cell wall in tissue context. To sterilize the seeds, they were rinsed with 100% EtOH for 15 s followed by double-distilled autoclaved water. The seeds were then stirred in 50% commercial bleach (1.44% final sodium hypochlorite concentration) for 5 min and washed 3-5 times with double-distilled autoclaved water. They were subsequently stratified at 4 °C for 3-4 days. The seeds were placed in sterile Petri plates containing 1× MS medium (Murashige & Skoog, 1962), 1% sucrose and 0.8% plant agar, and germinated under long-day (16 h) lighting. Seedlings used in this study were taken directly from Petri plates 2-5 days after germination.

Camellia japonica pollen was collected directly after anthesis from a plant grown in the greenhouse of the Montreal Botanical Garden. Pollen grains were then dehydrated over silica gel for 24 hours and stored at -20 °C until use. Pollen grains were hydrated for 30 min and suspended in a growth medium containing 0.1 mg/ml H_3BO_3, 0.3 mg/ml $Ca(NO_3)_2$, 0.1 mg/ml KNO_3, 0.2 mg/ml $MgSO_4$, and 80 mg/ml sucrose. Approximately 5 mg of pollen was added to 4 ml of growth medium in Erlenmeyer flasks and incubated at 25 °C under continuous slow shaking. For an illustrated guide on steps for pollen germination, refer to Chebli and Geitmann (2015).

Cell wall probes

Table 1 summarizes the sources of molecular probes and antibodies used in this study to label the cell wall polysaccharides.

Final version published in *Journal of Microscopy* doi.org/10.1111/jmi.12895

Methods

Fixation of pollen tubes

For immunolabeling, pollen tubes were fixed in 3.5% w/v formaldehyde freshly prepared by dissolving paraformaldehyde in Pipes buffer (50 mM Pipes, 1 mM EGTA, 0.5 mM $MgCl_2$, pH = 6.9). Fixation and rinsing steps were performed in a microwave (Pelco BioWave® 34700 with a Pelco ColdSpot®) at 150 W, 30±1 °C. The fixation was performed for 40 s, followed by 3 washes with Pipes buffer. For an illustrated guide to the fixation steps performed here refer to Chebli and Geitmann (2015).

Labeling of pollen tubes

Immunolabeling of pollen tubes

Monoclonal antibodies (mAbs) were used for immunofluorescence labeling of HG pectin and cellulose in fixed pollen tubes. Fixed samples were rinsed 3 times with PBS (135 mM NaCl, 3.2 mM Na_2HPO_4, 1.3 mM KCl, 0.5 mM KH_2PO_4, pH 7.3) containing 5% w/v Bovine Serum Albumin (BSA, Cedarlane). Fixed pollen tubes were incubated with the corresponding antibody diluted in PBS-BSA for 10 min under 20 in Hg vacuum in microwave operating at 150 W and 30±1 °C. Labeling was followed by 5 rinses with PBS-BSA buffer, each time for 40 s at 150 W and 30±1 °C. JIM5 and LM19 mAbs were used to label weakly esterified pectins (diluted 1:50). JIM7 and LM20 mAbs were used to label highly esterified pectins (diluted 1:50). The secondary antibody for JIM probes was Alexa Fluor 594 anti-rat IgG, diluted 1:100 (stock: 2 mg/ml). The secondary antibody for LM probes was Alexa Fluor 488 anti-rat IgM, diluted 1:100 (stock: 2 mg/ml). CBM3a was used to label crystalline cellulose and was diluted 1:100 (stock: 1 mg/ml) followed by incubation with mouse-anti-polyhistidine mAb diluted 1:12 (stock: 2 mg/ml), and subsequent incubation with Alexa Fluor 488 anti-mouse IgG diluted 1:100 (stock: 2 mg/ml). Following the labeling procedure, the samples were mounted on glass slides in a drop of Citifluor antifade AF1 (Electron Microscopy Sciences) for microscopic observation. For an illustrated guide to these steps refer to Chebli and Geitmann (2015). Tables 2 and 3 summarize the probes used here, their details and their targets.

Labeling of pollen tubes using COS^{488} and inorganic fluorophores

Labeling fixed pollen tubes

Labeling of pollen tubes using methods other than those based on antibodies was performed on both fixed and living samples. In case of fixed samples, staining for cellulose was performed by incubating the pollen tubes for 10 min with 0.5 mg/ml CFW in ddH_2O or with 8 µg/ml PFS in PBS. The PFS concentration used here to label the pollen tubes was based on previous studies (e.g., Lampugnani et al., 2013, Sede et al., 2018, Anderson et al., 2010), and is considerably lower than that used to label pavement cells of *Arabidopsis* cotyledons mentioned later. The higher concentration used for staining *Arabidopsis* seedlings helps overcoming penetration issues caused by the presence of the cuticle at the cotyledon surface. Pectin was labeled with 1:1000 COS^{488} diluted in 2-(N-morpholino) ethanesulfonic acid (MES) (Sigma Aldrich) buffer (25 mM, pH 5.7) (Mravec et al., 2014). The samples were then washed 5 times with PBS and mounted on glass slides in a drop of Citifluor antifade AF1 (Electron Microscopy Sciences). Tables 2 and 3 summarize the probes used, their targets and labeling details.

Final version published in *Journal of Microscopy* doi.org/10.1111/jmi.12895

Table 1. Fluorescent probes and antibodies used.

Fluorescent probe/antibodies	Source	Identifier
Propidium iodide (PI)	Sigma-Aldrich	Cat# P4170-100MG
Pontamine Fast Scarlet 4B (PFS)	Sigma-Aldrich	Cat# 212490-50G
Calcofluor white (CFW)	Sigma-Aldrich	Cat# F6259
COS^{488}	(Mravec et al., 2014)	-
JIM5	Plant Probes (Knox et al., 1990)	JIM5
JIM7	Plant probes (Knox et al., 1990)	JIM7
CBM3a	Plant Probes (Blake et al., 2006)	CBM3a
LM19	Plant Probes (Verhertbruggen et al., 2009)	LM19
LM20	Plant Probes (Verhertbruggen et al., 2009)	LM20
Mouse-anti-polyhistidine	Sigma-Aldrich	H1029-.2ML
Goat anti-rat IgG Alexa Fluor 594	Molecular Probes	A11007
Goat anti-rat IgM Alexa Fluor 488	Molecular Probes	A21212
Goat anti-mouse IgG Alexa Fluor 488	Molecular Probes	A11001

Labeling growing pollen tubes

Living pollen tubes were also labeled with PI, CFW and COS^{488}. To this end, pollen grains were first hydrated for 30 min, and then suspended in the growth medium. The suspension was injected into channels of a commercial fluidic microscopy channel slide, µ-Slide VI 0.4 (IBIDI GmbH). The microchannel slides were then left on the bench for an hour for pollen tubes to germinate. After germination, 30 µl of PI solution (0.1 or 1 mg/ml) was injected into each channel. For CFW, 2 µl of 0.1 mg/ml CFW dissolved in growth medium was injected into each channel containing 150 µl of pollen tube suspension, reaching a final concentration of 1.3 µg/ml. Similarly, COS^{488} was diluted 1:4 in growth medium and 2 µl of the solution was injected into each channel reaching a final concentration of 1:300. The microchips were tilted repeatedly to mix the injected label solution with the pollen suspension before microscopic observation. Tables 2 and 3 summarize the probes used, their targets and labeling details.

Final version published in *Journal of Microscopy* doi.org/10.1111/jmi.12895

Table 2. Summary of materials and methods used for fluorescence labeling of the cell wall in the present study.

	Fluorescent probe	Concentration	Incubation time	Target (putative)	Cells visualized	Live/Fixed
Dyes	Propidium iodide (PI)	0.01-1 mg/ml (in ddH_2O)	~7 min (on bench. For 0.5 mg/ml)	Pectin (affinity for de-esterfified GalA)	Root hairs, epidermal cells (root, shoot, cotyledon) (*AT*[1])	Live
		0.1 mg/ml (in ddH_2O)	Immediate*		Pollen tube (*CJ*[2])	Live
	Pontamine Fast Scarlet 4B (PFS)	0.14-14 mg/ml (in PBS)	45 min (rotator)	Cellulose	Root hairs, epidermal cells (root, shoot, cotyledon) (*AT*)	Live
		8 µg/ml (in PBS)	10 min (Vac[3] & MW[4])		Pollen tube (*CJ*)	Fixed
	Calcofluor white (CFW)	2-10 mg/ml (in ddH_2O)	~45-90 min (Vac and rotator)	β-glucans (cellulose, xyloglucans, callose, chitin)	Root hairs, epidermal cells (root, shoot, cotyledon) (*AT*)	Live
		0.5 mg/ml (in ddH_2O)	10 min (Vac & MW)		Pollen tube (*CJ*)	Fixed
		1.3 µg/ml (in growth medium)	Immediate*			Live
Oligo probe[5]	COS^{488**}	1:500 (in MES) (stock: 1 mg/ml)	5-15 min (rotator)	Very low DE[6] HG	Root hairs, epidermal cells (root, shoot, cotyledon) (*AT*)	Live
		1:1000 (in MES) (stock: 1 mg/ml)	10 min (Vac & MW)		Pollen tube (*CJ*)	Fixed
		1:300 (in growth medium)	Immediate*			Live
Primary antibodies[7]	JIM5	1:50 (in PBS-BSA) (stock: N/A[8])	10 min (Vac & MW)	Low DE HG (0-40%, peaks ~ DE 40%)[9]	Pollen tube (*CJ*)	Fixed
	JIM7	1:50 (in PBS-BSA) (stock: N/A[8])	10 min (Vac & MW)	High DE HG (15%-80%)[9]	Pollen tube (*CJ*)	Fixed
	LM19	1:50 (in PBS-BSA) (stock: N/A[8])	10 min (Vac & MW)	Low DE HG (?, <50%[10])	Pollen tube (*CJ*)	Fixed
	LM20	1:50 (in PBS-BSA) (stock: N/A[8])	10 min (Vac & MW)	High DE HG (?%)	Pollen tube (*CJ*)	Fixed
	CBM3a	1:100 (in PBS-BSA) (stock: 1 mg/ml)	10 min (Vac & MW)	Cellulose (crystalline), xyloglucan	Pollen tube (*CJ*)	Fixed

[1]*AT*: *Arabidopsis thaliana*, [2]*CJ: Camellia japonica*, [3]Vac: vacuum, [4]MW: microwave, [5]Oligo probe: oligosaccharide-based probe, [6]DE: degree of methyl-esterification, [7]Information related to secondary antibodies is

Final version published in *Journal of Microscopy* doi.org/10.1111/jmi.12895

presented in Table 3, [8]Stock concentration not provided by the supplier. [9]From Willats et al. (2000). [10]From Christiaens et al. (2011), for randomly esterified pectin.[*]Label was added to the fluidic channel and microscopy was performed from a few minutes to a few hours after that. [**] Chitosan oligosaccharide-base probe conjugated to Alexa Fluor 488.

Table 3. Secondary antibodies used.

	Fluorescent probe	Concentration	Incubation time	Target
Secondary antibodies	Mouse anti-Polyhistidine	1:12 (in PBS-BSA) (stock: 2 mg/ml)	10 min (Vac[1] & MW[2])	CBM3a
	Goat anti-rat IgG Alexa Fluor 594	1:100 (in PBS-BSA) (stock: 2 mg/ml)	10 min (Vac & MW)	JIM5 and JIM7
	Goat anti-rat IgM Alexa Fluor 488	1:100 (in PBS-BSA) (stock: 2 mg/ml)	10 min (Vac & MW)	LM19 and LM20
	Goat anti-mouse IgG Alexa Fluor 488	1:100 (in PBS-BSA) (stock: 2 mg/ml)	10 min (Vac & MW)	Anti-Polyhistidine

[1]Vac: vacuum, [2]MW: microwave

Labeling *Arabidopsis thaliana* seedlings

Arabidopsis seedlings were labeled without fixation. Seedlings were extracted directly from Petri plates and, unless otherwise stated, they were placed in Eppendorf tubes containing 1 ml of the labeling solution. Seedlings were kept physically intact during the labeling procedures. The tubes were covered with aluminum foil to minimize light exposure and all steps were performed under low light conditions. After incubation with the label, seedlings were rinsed 3-5 times using the same buffer used to dilute the respective label. Rinsing was performed immediately before imaging and by removing a seedling from the Eppendorf tube, placing it in a Petri plate and quickly covering it with several drops of the rinsing solution. The rinsing solution was gently circulated over the sample using a disposable pipette and then replaced with fresh solution after 30 s. Rinsing is a critical step to remove excess or unbound fluorophores which allows minimizing background noise. The mounting media were the same as the ones used to dilute the respective label.

Staining *Arabidopsis thaliana* seedlings for cellulose

To stain for cellulose, CFW and PFS were used. CFW was diluted in ddH_2O at concentrations of 2-10 mg/ml. All concentrations in this range were found to produce satisfactory outcomes. To promote dye penetration, the open Eppendorf tubes can be placed under a mild vacuum (~ 20 in Hg) for about 45 min followed by a 45 min incubation on a rotator in the dark before rinsing and microscopy, as performed by Bidhendi et al. (2019). The vacuum infiltration step can be omitted depending on sample type and success of dye penetration. The samples were then unmounted from the rotator and kept in the dark until rinsing and visualization. PFS was diluted in PBS buffer at concentrations of 0.14-14 mg/ml. The samples were placed in Eppendorf tubes containing 1 ml of diluted dye and mounted on a

Final version published in *Journal of Microscopy* doi.org/10.1111/jmi.12895

rotator for 45 min prior to observation. It should be noted that these protocols were originally developed to observe the outlines and specifically the orientation of cellulose microfibrils (or cellulose bundles) in cotyledon pavement cells which are covered by a cuticle (Bidhendi et al., 2019). Therefore, the incubation times and/or the concentrations mentioned here can be substantially reduced for other organs devoid of a cuticle or those that are highly absorbent, such as the root. Tables 2 and 3 summarize the probes used, their targets and labeling details.

Labeling *Arabidopsis thaliana* seedlings for pectin

For labeling pectin in pavement cells, seedlings were incubated with either COS^{488} or PI. COS^{488} was diluted 1:500 (stock: 1 mg/ml) in MES buffer (25 mM, pH 5.7). The seedlings were incubated in 1 ml of COS^{488} in Eppendorf tubes for 5-15 min on a rotator and were then rinsed with MES. PI was found to readily and rapidly stain the cell walls of *Arabidopsis* seedlings. For the purpose of staining the epidermal layer, we found it to be generally sufficient to cover the seedling with only one or two drops of the PI solution. For this purpose, each seedling was removed from the cultivation Petri plates, placed in a new Petri plate used as staining container and covered immediately with one or two drops of PI. The Petri plate was then closed and placed inside a box to minimize light exposure. We found that a wide range of PI concentrations (0.01-1 mg/ml, diluted in ddH_2O) can properly stain pavement cells, allowing visualization of cell outlines. While for live-cell imaging, low concentrations of any labels are generally preferable to minimize the probability of cell toxicity, for one-time imaging of the seedlings, we used a 0.5 mg/ml PI concentration. Samples incubated for about 7 min showed strong staining. Interestingly, we observed that considerably longer incubation times (>20 min) had diminishing effects on signal strength. For rinsing, PI drops can be removed from the samples, using either a disposable pipette or an absorbent tissue paper, and replaced quickly with ddH_2O. Tables 2 and 3 summarize the probes used here, their targets and labeling details.

Confocal microscopy

Fluorescence and differential interference contrast (DIC) micrographs were acquired using a Zeiss LSM 710 confocal microscope unless specified otherwise. The excitation wavelengths and emission windows used were 405 nm and 410-523 nm for CFW, 514 nm and 520-650 nm for PFS, 488 nm and 510-610 nm for COS^{488}, respectively. For Alexa Fluor 488, excitation wavelength and emission window of 488 nm and 493-630 nm were used, respectively. For Alexa Fluor 594, excitation wavelength and emission window of 594 nm and 599-734 nm were used, respectively. Some images were acquired on a Zeiss LSM 510 META confocal microscope using excitation wavelengths and emission windows 532 nm and 550-615 nm for PFS and PI, 489 nm and 550-615 nm for COS^{488}, and 405 nm and 420-480 nm in META mode for CFW, respectively (Figs. 1F,H,I; 2H,I,J,L; 3; 4). Scanning was performed unidirectionally with frame averaging equal to 2 (on LSM 710). To optimize image acquisition, especially for visualization of cellulose microfibrils, a number of parameters can be adjusted. Proper sample staining is crucial as sufficiently bright, uniform and specific staining generates adequate contrast between different structures. This also eliminates the need for using a higher gain value which can otherwise be used to amplify the signal but increases the background noise. Higher gain values may be necessary to reduce exposure time, for instance for live cell

Final version published in *Journal of Microscopy* doi.org/10.1111/jmi.12895

imaging. Decreasing the pinhole size approaching values close to an airy unit is generally desirable to remove out of focus signal but this parameter needs to be adjusted without eliminating relevant features. Scanning resolution is related to the number of pixels constituting the image. Higher resolution scanning allows a refined image with smaller pixels at the expense of increasing the scanning time. While lower scanning speed can provide better quality images, increasing exposure time can lead to phototoxicity in samples or bleaching of the fluorescence signal for some fluorophores. These parameters inevitably constitute a trade-off and need to be balanced for best image quality. Lastly, the quality of the objective lens determines image quality depending on magnification and numerical aperture. We used several objectives, namely, Plan-Apochromat 20×/0.8, 40×/1.4 oil, and 63×/1.4 oil objectives. Time lapse imaging of growing pollen tubes stained with CFW was performed on a spinning disk confocal microscope (Movie 1) (Yokogawa CSU X1 mounted on a Zeiss Axio Observer Z1). Time lapse imaging of growing pollen tubes labeled with COS^{488} was performed on LSM 710 system (Movie 2). Pre- and post-processing techniques such as image deconvolution or Airyscan microscopy (Huff et al., 2017, Zanella et al., 2013) can be used to acquire or enhance the quality of micrographs but these were not implemented for image acquisition in the present study.

Image analysis and processing

Analysis and preparation of fluorescence micrographs in this study were performed using the ImageJ distribution Fiji (Fiji Is Just ImageJ) (Schindelin et al., 2012), Zen 3.0 (Carl Zeiss microscopy GmbH) software. Fiji is capable of opening and analyzing the .lsm and the newer .czi file formats created by the Zeiss image acquisition software. Bio-Formats interface was used by Fiji/ImageJ to import proprietary file formats (https://www.openmicroscopy.org/bio-formats). For assessment of confocal data and 3D reconstruction (e.g., Fig. 1D), Imaris 9.5 (Bitplane) software was used. Confocal z-stacks were converted to .ims file format prior to visualizations in Imaris. Enhancement of fluorescence micrographs in this study was limited to moderate contrast and brightness adjustments in Fiji.

Results and Discussion

Staining roots of *Arabidopsis thaliana* seedlings for cellulose

Root hairs are tiny tubular extensions from root trichoblasts that increase the overall contact surface of the root and augment the plant's efficiency to absorb water and nutrients. The root hair is among the models used to investigate tip growth in plant cells (Carol & Dolan, 2002, Rounds & Bezanilla, 2013). Using electron microscopy, cellulose microfibrils are suggested to be short and randomly oriented in the newest cell wall deposited at apical region of the root hair allowing cell expansion at the tip, while an inner cell wall layer deposited in more mature regions of the hair contains well-ordered cellulose microfibrils restricting further expansion (Newcomb & Bonnett, 1965, Akkerman et al., 2012, Mendrinna & Persson, 2015). Staining whole seedlings using the protocols provided for CFW and PFS dyes allowed us to visualize the cellulose-like polysaccharides in the cell walls of the root hairs which are formed in the maturation zone of the root. Both stains were observed to label the entire profile of root hairs (Figs. 1A-C and 2A-D).

Final version published in *Journal of Microscopy* doi.org/10.1111/jmi.12895

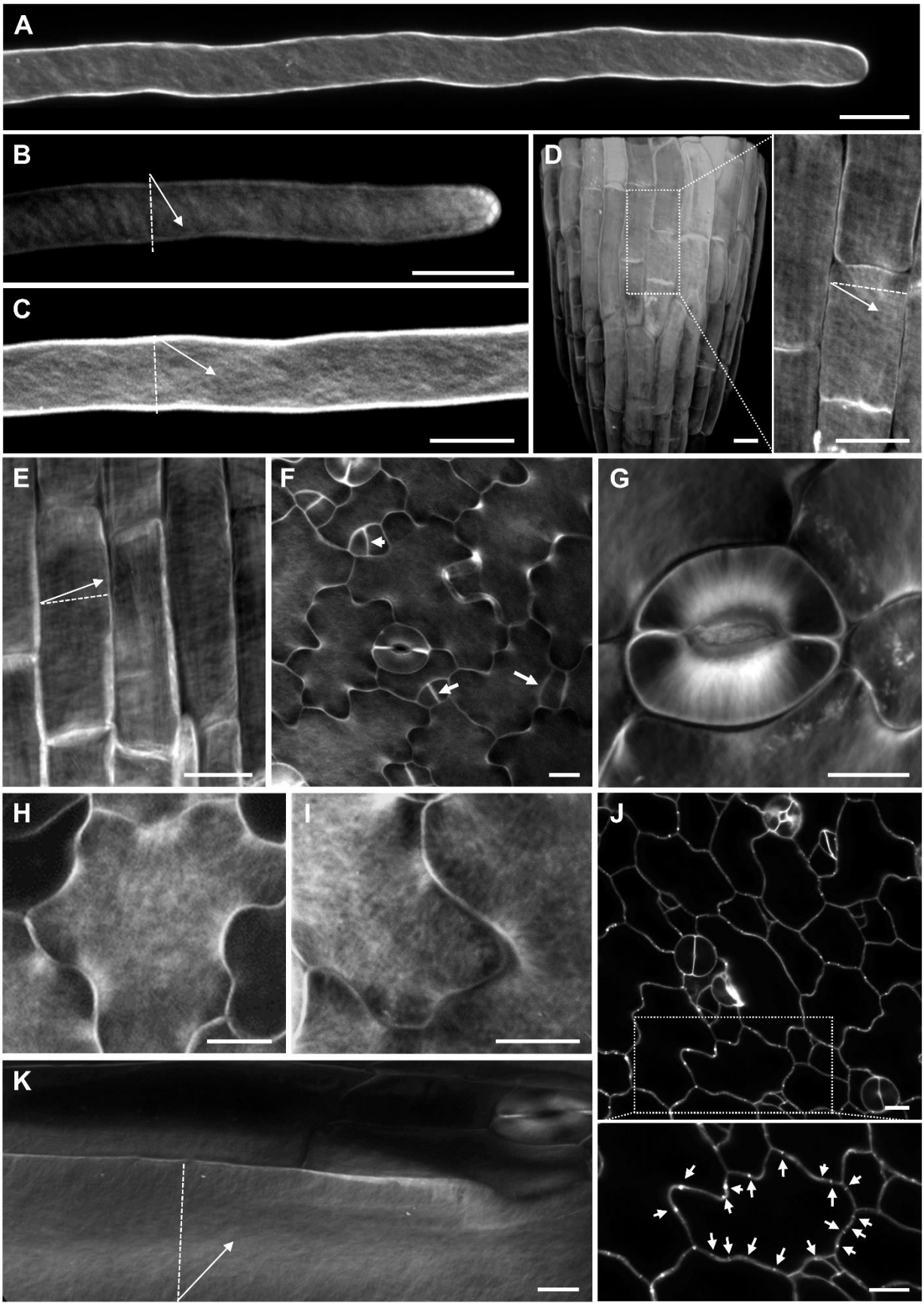

Final version published in *Journal of Microscopy* doi.org/10.1111/jmi.12895

Fig 1. Staining *Arabidopsis* seedlings with calcofluor white (CFW). A) Root hairs show fluorescent signal along their entire length (maximum projection)**, B)** with some displaying higher signal intensity at the tip (maximum projection of half of cylinder). **C)** The angle of the helical cellulose microfibril orientation varies between shallow **(B)** and steep **(C)** (maximum projection, shank of a root hair). **D)** Left: 3D reconstruction from z-stack micrographs of entire root tip. Right: magnified view of the selected region with maximum signal projection of epidermis cells only. **E)** Epidermal cells in the elongation zone of the root (maximum projection). **F)** Epidermal cells of the cotyledon (maximum projection). Intense label can be seen at newly deposited walls between dividing daughter cells (arrows). **G)** Close-up of a pair of guard cells showing a predominantly radial cellulose microfibril orientation (single optical section). **H)** Close-up of a cotyledon pavement cell demonstrating accumulation of cellulose at necks of border waves (maximum projection). **I)** Close-up of a border wave demonstrating radially diverging cellulose microfibrils at necks. Lobe tips typically exhibit lower signal intensity compared to necks. **J)** Top: CFW also binds callose, here revealing some of the plasmodesmata at borders of cotyledon pavement cells. Bottom: Close up of a pavement cell with arrows pointing at plasmodesmata (single optical section). **K)** Hypocotyl epidermal cells (maximum projection of few optical sections). The CFW concentration used for staining was 10 mg/ml, except for F, H, I where a concentration of 2 mg/ml was used. Dotted lines mark the transverse axes of the cells. Arrows indicate apparent orientation of cellulose microfibrils. The thickness of z-stacks used for maximum projections are 23.2 µm (A), 5.95 µm (B), 13.9 µm (C), 3.9 µm (for magnified view) (D), 2.3 µm (E), 7.25 µm (F), 3.3 µm (G), 10.8 µm (H), 4.84 µm (I), 0.33 µm (single section) (J) and 16.5 µm (K). Scale bars = 10 µm.

Some root hairs demonstrated higher signal intensity at the apical region (Figs. 1B, 2A-C), but this trend was not observed in all root hairs. These observations are consistent with the study by Park et al. (2011) where, using CBM3a and PFS, it was shown that cellulose-like polysaccharides are enriched at the apical region of growing root tips, in particular in younger root hairs. In some cases, with our staining protocol for CFW, we discerned cellulose bundles to have a distinct helical orientation in the shank of root hairs with an angle that varied between individual hairs (e.g., see Fig. 1A-C). We did not assess whether the root hairs continued growing under the experimental conditions. Should future experimentation demonstrate that this is the case, at the appropriate concentrations, CFW may be used for live imaging of cell wall dynamics during root hair growth. Similarly, PFS staining in some root hairs revealed cellulose microfibril orientation (Fig. 2D), however less discernible compared to CFW staining.

With our protocols for PFS and CFW staining, root epidermal cells were labeled strongly. At root tips and in the elongation zone, cellulose microfibril orientation was evident in epidermal cells (Figs. 1D,E and 2E-G). The observed oblique orientation of cellulose microfibrils closely matches the observations of cellulose microfibril orientation in root epidermal cells in *Lemna minor* L. and *Arabidopsis* visualized using either CFW or PFS (Inada et al., 2000, Anderson et al., 2010). Anderson et al. (2010) had shown the application of PFS in real-time imaging revealing the passive reorientation of the cellulose bundles in walls of longitudinally expanding cells.

Staining cellulose in aerial organs of *Arabidopsis*

Some of the most geometrically intriguing plant cell shapes are formed in the leaf epidermis. The simple cube-shaped cells generated in the

Final version published in *Journal of Microscopy* doi.org/10.1111/jmi.12895

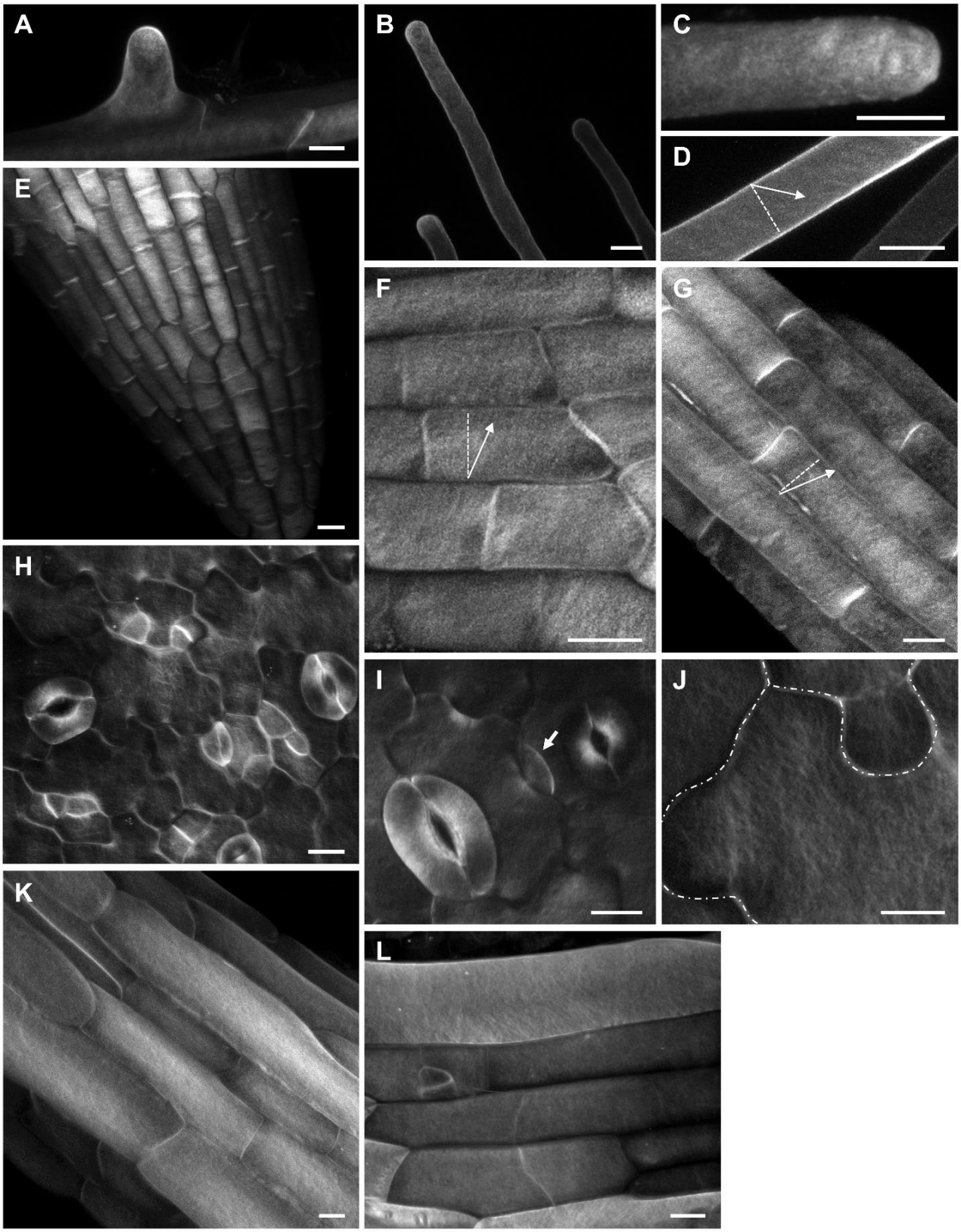

Final version published in *Journal of Microscopy* doi.org/10.1111/jmi.12895

Fig 2. Staining *Arabidopsis* seedlings with Pontamine Fast Scarlet 4B (PFS). A) Emerging and **B)** elongated root hairs, some displaying signal at the tip. **C)** Close-up of a root hair displaying signal at the tip. **D)** Cellulose microfibril orientation is apparent in the shank of a root hair. **E)** Epidermis cells close to the root tip. **F)** Close-up of root tip epidermal cells. **G)** Epidermal cells of the root elongation zone. **H)** Cotyledon epidermal cells. **I)** Guard cells showing a radial pattern of cellulose microfibrils emanating from the pore periphery. Newly deposited walls between dividing daughter cells are labeled (arrow). **J)** Cotyledon epidermal cells showing the abundance of label at sites of indentations (necks) while signal at tip of protrusions (lobes) is weaker. The dash-dotted lines demarcate the cell borders. **K)** Hypocotyl epidermal cells. **L)** Close-up view of a hypocotyl epidermal cells. All micrographs are maximum projections. PFS concentration was 0.14 mg/ml (A), 1.4 mg/ml (B, E), and 14 mg/ml (C, D, F, G, H, I, J, K, L) for the rest of images. Dotted lines mark the transverse axes of the cells. Arrows indicate apparent orientation of cellulose microfibrils. The thickness of z-stacks used for maximum projections are 26.3 µm (A), 57.3 µm (B), 30.5 µm (C), 54.3 µm (D), 48.8 µm (E), 3.5 µm (F), 54.6 µm (G), 5.8 µm (H), 4.8 µm (I), 9.9 µm (J), 22.6 µm (K) and 11.5 µm (L). Scale bars = 10 µm.

outermost layer of the shoot apical meristem develop into cells as differently shaped as trichomes, guard cells and pavement cells. Pavement cells of many plant species develop to form an interlocking jigsaw puzzle-shaped pattern that demonstrates a varying degree of waviness at cell borders (Vőfély et al., 2019, Panteris & Galatis, 2005). Compressive mechanical stresses in the anticlinal cell walls leading to buckling are suggested to underlie the formation of these undulating shapes, in tandem with a feedback loop that locally reinforces the cell wall at the location of indents by deposition of cellulose and de-esterification of pectin (Bidhendi et al., 2019). In dicotyledons, pairs of kidney-shaped guard cells form stomatal pores. Various cell wall polysaccharides have been proposed to play a role both in the morphogenesis and functioning of these cells, including radially deposited bundles of cellulose microfibrils and the de-esterification of HG pectin at cell poles (Carter et al., 2017, Rui et al., 2019, Yi et al., 2018, Palevitz & Hepler, 1976, Galatis & Mitrakos, 1980, Aylor et al., 1973). The proposed staining protocols using CFW and PFS allowed us to visualize cellulose in epidermal pavement and guard cells. Both stains showed higher signal in the indented (neck) regions of the pavement cell border waves where fibrillar bundles fan into the periclinal walls. On the opposing side, in the lobe of the neighboring cell, cellulose bundles assumed a transverse orientation, similar to the spatial configuration that characterized the guard cells (Figs. 1F-I and 2H-J). In both cell types, label was scarce at cell tips. In mature guard cells, both stains showed a radial pattern of cellulose bundles (Figs. 1G and 2I). Both CFW and PFS stains were enriched at the newly deposited cell walls separating dividing cells (Figs. 1F and 2H,I), consistent with the notion that cell plates, the precursors of these new walls, contain cellulose at later developmental stages (Drakakaki, 2015, Gu et al., 2016). CFW, but not PFS, was also observed to mark plasmodesmatal structures in pavement cells (Fig. 1J). This is presumably because CFW also stains the cell wall polymer callose known to be associated with plasmodesmatal channels (De Storme & Geelen, 2014). However, this does not preclude the possibility that these structures can contain cellulose or pectin as well. Both PFS and CFW stained hypocotyl epidermal cells despite the presence of a cuticle (Figs. 1K and 2K,L) although dye penetration was often not as uniform as in the other organs.

Final version published in *Journal of Microscopy* doi.org/10.1111/jmi.12895

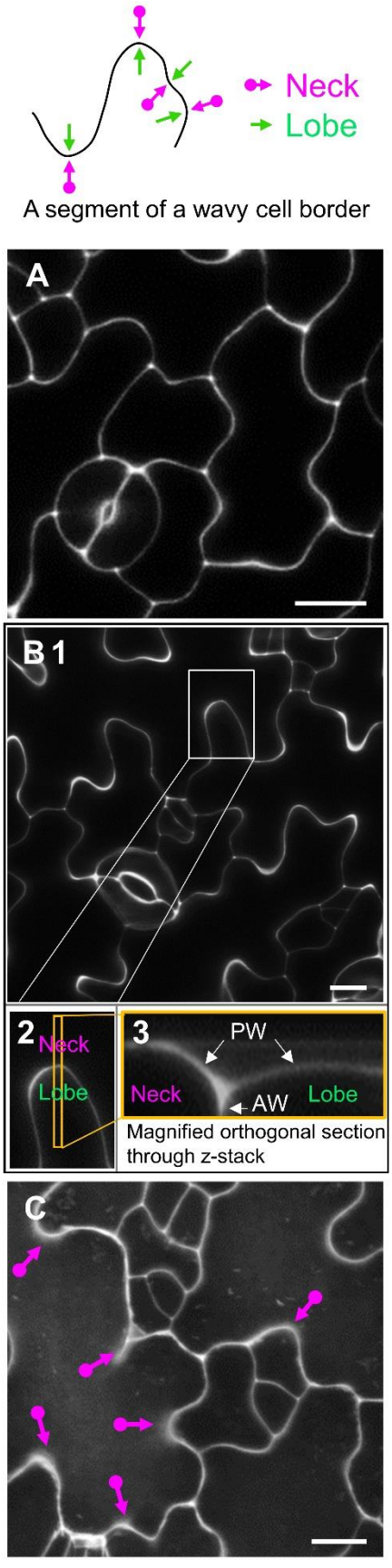

Fig 3. Labeling *Arabidopsis* cotyledon pavement cells with COS^{488}. Pavement cells of cotyledons and leaves in many plant species demonstrate wavy borders with interlocking indents (necks, magenta arrow) and protrusions (lobes, green arrow). **A)** Tricellular junctions are brightly labeled (single optical section). **B) 1)** Signal intensity fluctuates along the undulating border of pavement cells (single optical section). **2)** Close-up of a lobe/neck pair from (**1**). **3)** A slice of the reconstructed stack showing the lobe/neck pair of (**2**) from orthogonal view. The slice shows that periclinal (PW) and anticlinal (AW) walls are both labeled. It further shows that, as discussed by Bidhendi et al. (2019), the neck periclinal wall exhibits a higher signal intensity and bulges out above the lobe side periclinal wall. **C)** Maximum projection of z-stack shows higher signal intensity associated with the periclinal walls at the necks (arrows). The thickness of optical sections and the thickness of z-stack used for maximum projection are 0.44 µm (A), 0.3 µm (B) and 13.8 µm (C). Scale bars = 10 µm.

The simple protocols provided here for CFW and PFS staining of *Arabidopsis* seedlings, allow visualization of the spatial distribution, and in most cell types, the orientation of cellulose microfibrils. PFS staining results were largely consistent with CFW results. The staining was also observed to increase with incubation time. Since samples were not fixed, excessive incubation times resulted in collapsed cells. Therefore, the incubation time cannot be increased unboundedly.

Labeling epidermal pavement cells for pectin

Pectin is an important component of most primary plant cell walls and is also enriched in the middle lamella, the thin layer of material that glues plant cells together (Zamil & Geitmann, 2017). To label pectin in the epidermis of *Arabidopsis* cotyledons,

Final version published in *Journal of Microscopy* doi.org/10.1111/jmi.12895

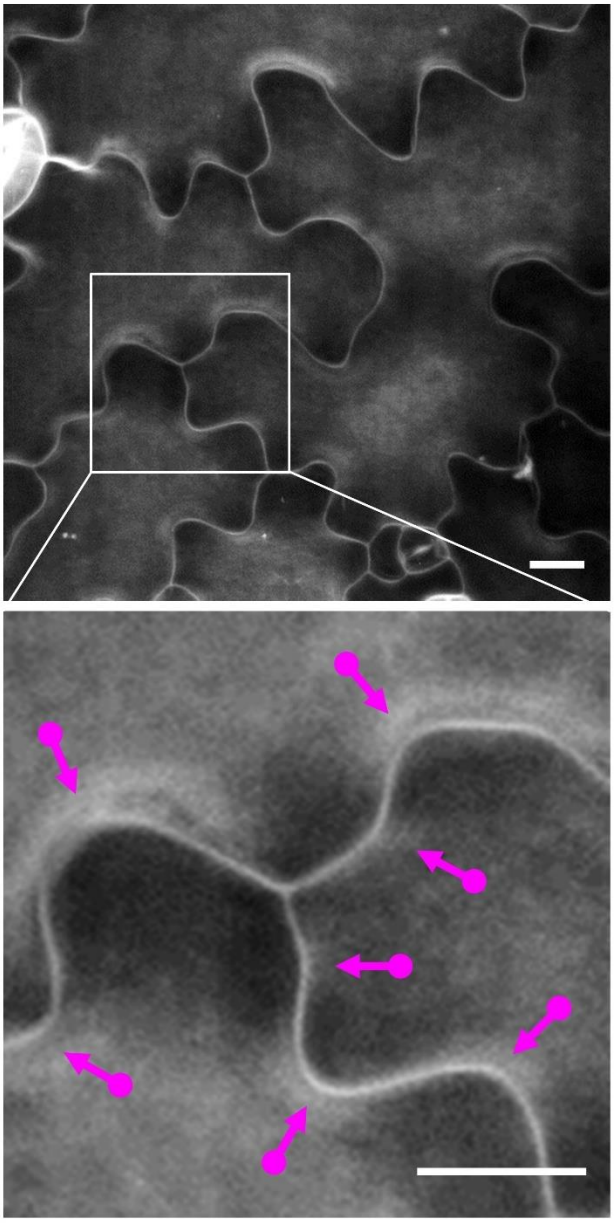

Fig 4. Staining *Arabidopsis* cotyledon pavement cells with propidium Iodide (PI). Maximum projection of z-stack shows higher signals associated with necks. Bottom figure is a magnified view of the boxed region with arrows pointing at necks that, regardless of their curvature, consistently demonstrate a higher signal than lobes. Concentration of PI used to obtain this micrograph was 0.5 mg/ml. The thickness of the z-stack used for maximum projection is 26.4 μm (C). Scale bars = 10 μm.

we used either COS^{488} or PI. COS^{488} is suggested to bind weakly esterified pectin (Mravec et al., 2014). Labeling cotyledons using COS^{488} revealed fluorescent label in anticlinal and periclinal walls of pavement and guard cells (Fig 3, see also the orthogonal view in Fig. 3B). In addition, strong label was associated with tricellular junctions, consistent with the de-esterified pectin-enrichment of the middle lamella (Fig. 3A). On single optical sections, the intensity of the fluorescence signal fluctuated along the undulating anticlinal walls in wavy pavement cells (Fig. 3B). From maximum projections of z-stacks it is obvious that neck sides of undulations demonstrate higher COS^{488} signal in the periclinal wall (arrows in Fig. 3C). Because COS^{488} binds with weakly esterified pectin, we had posited that necks are sites where HG pectin is prone to gel formation through calcium bridging resulting in stiffening of the cell wall matrix (Bidhendi et al., 2019, Bidhendi & Geitmann, 2016).

Rounds et al. (2011) suggested that PI binds demethylesterified GalA residues. Consistent with COS^{488} labeling, upon staining of cotyledon pavement cells using PI we observed neck regions of undulating pavement cells to exhibit higher signal in the indentation sides of the waves on the periclinal wall (Fig. 4A) (Bidhendi et al., 2019). When used at low concentrations (e.g., 0.01 mg/ml), PI is also suitable for time-lapse imaging of expanding pavement cells (Bidhendi et al., 2019).

The proposed protocols for COS^{488} and PI were able to label epidermal cells of *Arabidopsis* cotyledon. PI is a dye that allows for the rapid fluorescent staining of plant cells with minimal sample preparation required. However, there is much left to be explored about its cell wall binding behavior or, in general, about its interaction with plant cells. Further studies are required to evaluate

Final version published in *Journal of Microscopy* doi.org/10.1111/jmi.12895

the usefulness of PI in live imaging of different plant cell types and its binding specificity for different cell wall components.

Labeling fixed pollen tubes for cellulose

Pollen tubes are cylindrical protuberances produced by pollen grains. They serve to deliver the sperm cells to a receptive ovule as a step in the sexual reproduction of seed plants (Chebli & Geitmann, 2007). Pollen tube elongation is accomplished through a highly regulated polar growth process similar to that of root hairs (Geitmann & Dumais, 2009). Due to its rapid growth, simple geometry, and ease of in vitro cultivation, the pollen tube is a widely used model to investigate cell growth and cell wall modification in plant cells (Geitmann, 2010a) and to test the binding of cell wall probes (Mravec et al., 2017).

The pollen tube wall contains both cellulose and callose (Aouar et al., 2010, Chebli et al., 2012) and the use of CFW alone does not allow to distinguish these. CFW staining of *Camellia* pollen tubes revealed a gradient of signal intensity from the base toward the tip of pollen tubes (Fig. 5A). This distal-apical signal gradient is consistent with the results reported for *Arabidopsis* pollen tubes stained with CFW (Marković et al., 2019). Signal at the tip was absent in some cells and present in others. Other studies found less variability between cells, but results are somewhat inconsistent between studies. Mravec et al. (2017) showed the tip of *Arabidopsis* pollen tubes to be devoid of CFW signal, whereas Dardelle et al. (2010) showed the presence of CFW signal at the tip of *Arabidopsis* pollen tubes. In other plant species, CFW label at the tip is more consistently present or absent within a pollen population. *Lilium* pollen tubes show consistently prominent label at the tip (Aouar et al., 2010, Fayant et al., 2010), whereas in *Solanum* label was absent at the tip (Aouar et al., 2010). CFW also marks callose plugs in pollen tubes (Fig. 5B) and whether or not this signal indicates that next to callose these structures contain cellulose (Ferguson et al., 1998) requires the use of a more specific labeling strategy. Aniline blue which specifically binds callose is useful in that regard (Aouar et al., 2010, Parre & Geitmann, 2005). With PFS label, many *Camellia* pollen tubes showed a longitudinal signal gradient, although some tubes displayed label at the tip, as discussed for CFW staining (Fig. 5C,D). Similar results had been obtained with PFS and CFW in *Arabidopsis* (Sede et al., 2018) and *Picea meyeri* (Chen et al., 2009), respectively.

Using CBM3a that binds crystalline cellulose, but also xyloglucans (Hernandez-Gomez et al., 2015), yielded non-uniform results within a population of *Camellia* pollen tubes. Some tubes displayed signal all along the profile of the pollen tube (Fig. 5E), whereas in others the apex lacked signal (Fig. 5F). This variability is consistent with data reported for *Arabidopsis* pollen tubes (Chebli et al., 2012, Zhang et al., 2016). Using CBM3a, Parrotta et al. (2019) suggest crystalline cellulose to be present everywhere along the pollen tube profile but with a punctate distribution and less abundantly at the tip, a pattern that seemed to be altered by cold stress. Staining pollen tubes of *Nicotiana alata* using PFS, Lampugnani et al. (2013) suggested pollen tubes to display signal at the tip at early growth stages (4 h) and the signal to shift behind the apex in later stages of growth (16 h), an effect that is reminiscent of the phenomena observed in root hairs. Regardless of these variabilities, the experimental protocols presented here for PFS, CFW and the CBM3a showed to be successful in labeling fixed pollen tubes for cellulose. Further, importantly, the

Final version published in *Journal of Microscopy* doi.org/10.1111/jmi.12895

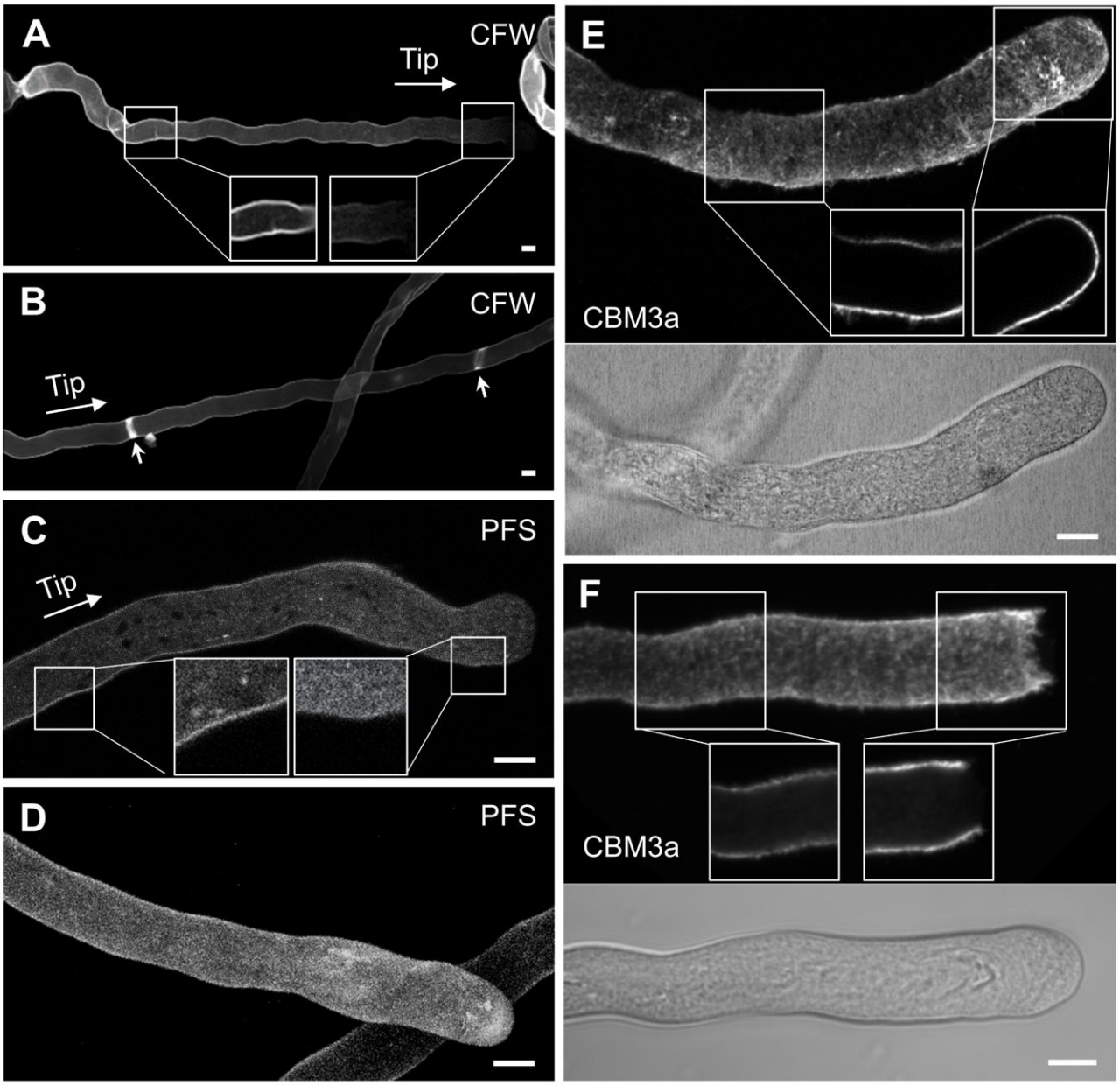

Fig 5. Labeling *Camellia japonica* pollen tubes with calcofluor white (CFW), Pontamine Fast Scarlet 4B (PFS) and Carbohydrate Binding Module 3a (CBM3a). A) CFW stain demonstrates a longitudinal gradient, with decreasing signal intensity toward the apex of the pollen tube. **B)** CFW marks callose plugs. **C)** PFS staining demonstrates a signal that typically decreases toward the tip, but exceptions exist (**D)**. (**E**) CBM3a labeling shows signal in all regions including the apex in some pollen tubes but not in others (**F**). Main fluorescent images are all maximum projections of z-stacks, insets are single optical sections for the boxed regions. DIC micrographs are provided to illustrate cell outlines. The thickness of z-stacks used for maximum projections and/or the single optical sections are 15.3 and 0.9 μm (optical section) (A), 17.9 μm (B), 37.1 and 0.64 μm (optical section) (C), 34.5 μm (D), 38.7 μm and 0.74 μm (optical section) (E) and 25 and 0.5 μm (optical section) (F). Scale bars = 10 μm.

Final version published in *Journal of Microscopy* doi.org/10.1111/jmi.12895

results illustrate the highly dynamic nature of cell wall distribution in pollen tubes that may dramatically change not only based on growth conditions such as the composition and osmolarity of the growth media (Biagini et al., 2014), but also based on the instantaneous growth rate and the stage of development. This emphasizes the importance of live labeling and real-time imaging of cell wall composition and reiterates that conclusions drawn from snapshot images of pollen tubes may not provide the full picture.

Labeling fixed pollen tubes for pectin

Labeling for pectin performed using COS^{488} showed a decreasing signal gradient towards the tip of pollen tubes (Figs. 6A,B). This result closely matches the labeling of live pollen tubes using OG7-13, another newly introduced oligosaccharide-based probe suggested to bind weakly esterified pectin in the presence of exogenous calcium (Mravec et al., 2017).

Our label with JIM5 and LM19 monoclonal antibodies specific to weakly esterified pectins (Hervé et al., 2011, Knox et al., 1990) showed a similar longitudinal gradient (Figs. 6C,D). Label for esterified pectins using JIM7 and LM20 showed signal confined mostly to the apical region of the pollen tubes (Figs. 6E,F). These results obtained with *Camellia* pollen tubes in the present study are consistent with previous studies using mAbs for HG on pollen tubes of various species (Chebli et al., 2013, Chebli et al., 2012, Dardelle et al., 2010, Wang et al., 2013, Parre & Geitmann, 2005, Fabrice et al., 2018, Leszczuk et al., 2019). Taken together, our proposed protocols for labeling fixed pollen tubes with cell wall specific antibodies or staining with inorganic fluorophores resulted in reproducible results for the distribution of esterified and de-esterified HG pectin. Slight differences between the patterns of COS^{488} labeling and the JIM5 or LM19 label are likely caused by the differing specificity for the degree of pectin esterification of these agents (Mravec et al., 2017, Verhertbruggen et al., 2009), reflecting, in part, the gradually changing activity of pectin-methyl esterases (PME) along the length of the pollen tube (Röckel et al., 2008).

Labeling live pollen tubes

As discussed in previous sections, at least for the fast-growing cells such as pollen tubes, time-lapse imaging of cell wall dynamics can reveal developmental details that are not evident from single snapshots obtained from different samples or even from distant time points of the same sample. To track cell wall dynamics, the use of labels that do not require fixation and do not interfere with cell growth is fundamental. For evaluation purposes, we labeled live pollen tubes using PI, CFW and COS^{488}. We used two different concentrations of PI to stain growing *Camellia* pollen tubes yielding label along the entire cell profile. In some but not all pollen tubes, the signal appeared to be stronger over a limited region at the tip (Fig. 7A) matching data by Rounds et al. (2011). This pattern, however, does not match the signal gradient for labels presented for HG pectin, and particularly that of labels for de-esterified pectin (JIM5 and LM19). Further, the region with relatively stronger label was not always limited to the tip and could occur on locations on the shank as well (Fig. 7B). Interestingly, PI staining was also observed at callose plugs (Fig. 7C) corroborating the putative presence of de-esterified pectin in these structures (Hasegawa et al., 2000). Clearly, the mechanisms of binding and the molecular targets of PI in the cell wall of pollen tubes require further investigation. We found that pollen tubes could continue growing in

Final version published in *Journal of Microscopy* doi.org/10.1111/jmi.12895

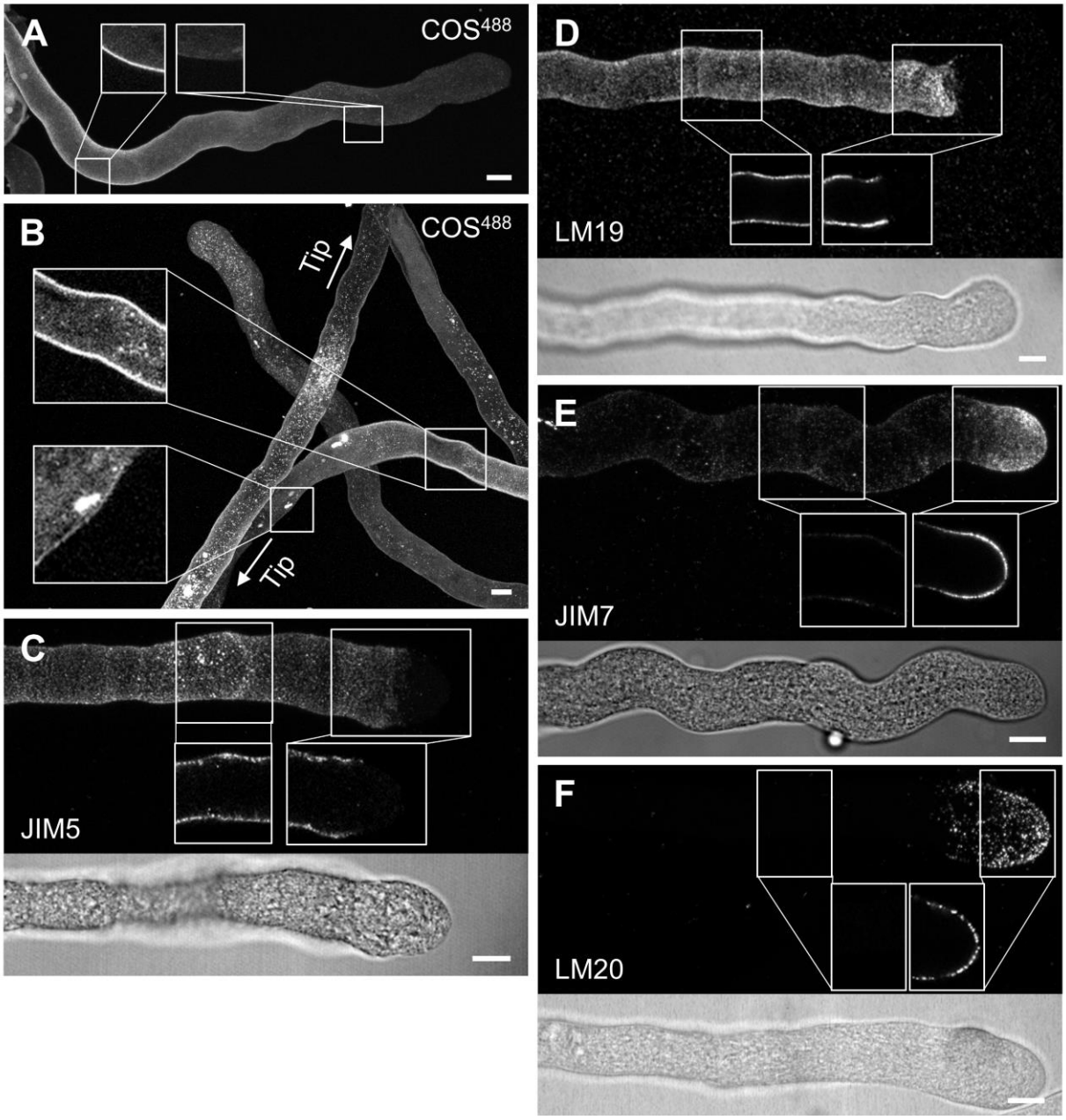

Fig 6. Labeling *Camellia japonica* pollen tubes for pectin. A) and B) Cos[488] labeling of fixed pollen tubes demonstrates higher signal intensity in the shank of pollen tubes, decreasing towards the tip. Punctate cytoplasmic label appears to be associated with organelles. The insets present magnified views to illustrate the decreasing signal gradient towards the apical region. **C)** JIM5 and **D)** LM19 label for de-esterified pectin showing higher signal in the distal parts of the pollen tube and weaker signal in the apical region. Label with **E)** JIM7 and **F)** LM20 for esterified pectin displaying higher signal at the apical region. All main figures are maximum projections, figure insets are single optical sections for the boxed regions. Corresponding DIC micrographs are provided to illustrate cell outlines. The thickness of z-stacks used for maximum projections and/or the single optical sections are 48.6 and 0.65 µm (optical section) (A), 59.2 and 0.66 µm (optical section) (B), 28.5 and 0.7 µm (optical section) (C), 47.8 and 0.64 µm (optical section) (D), 35.6 and 0.7 µm (optical section) (E) and 28.3 and 0.74 µm (optical section) (F). Scale bars = 10 µm.

Final version published in *Journal of Microscopy* doi.org/10.1111/jmi.12895

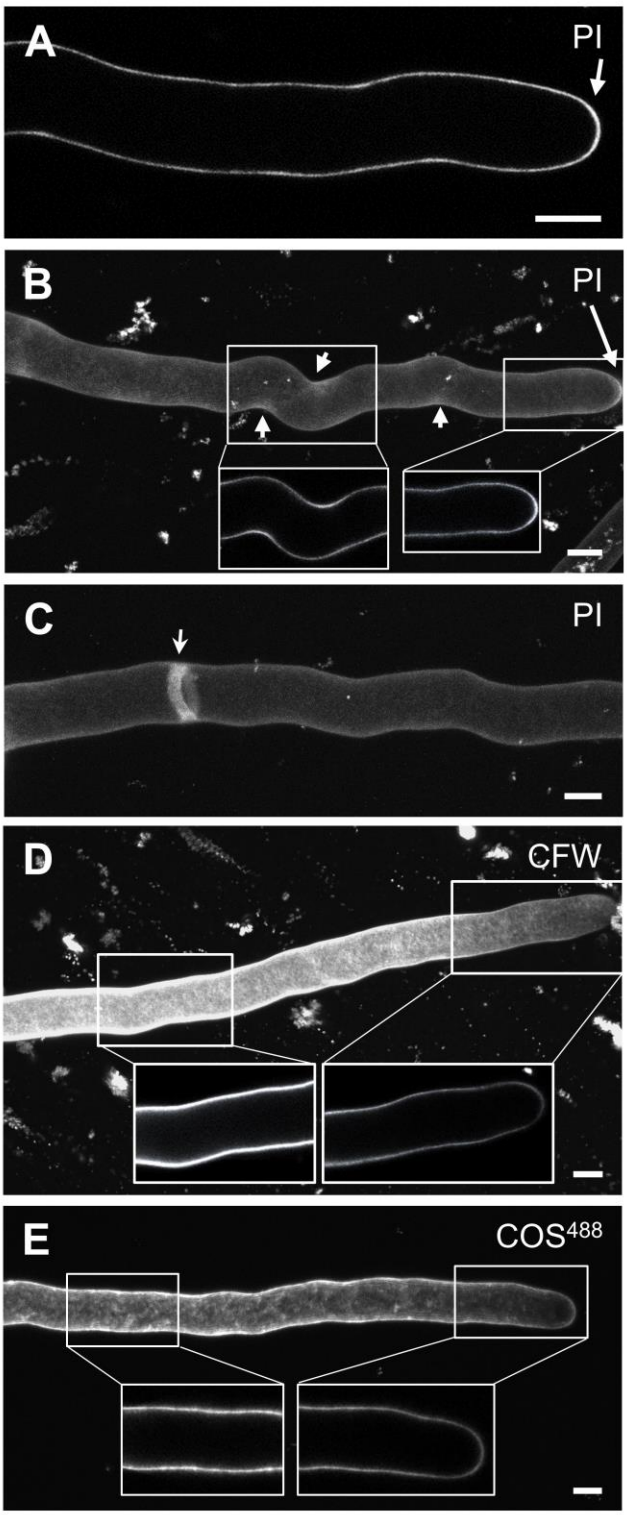

Fig 7. Live labeling of growing *Camellia japonica* pollen tubes germinating in channels of a microscope slide (µ-Slide VI 0.4, IBIDI GmbH). A) Propidium iodide (PI) staining of growing pollen tube cell wall (single optical section). In many pollen tubes, the signal appears stronger at the tip (arrow). **B)** Higher PI signal is associated with the concave sides of bends in some pollen tubes (maximum projection). **C)** PI stain is associated with callose plugs (maximum projection). **D)** Calcofluor white (CFW) staining of living pollen tubes. Pollen tubes continued growing up to several hours after staining. A decreasing signal gradient towards the apical region could be observed (maximum projection, also see Movie 1). **E)** COS^{488} labeling of growing pollen tubes. Pollen tubes continued growing up to several hours after labeling (maximum projection, also see Movie 2). All figure insets are single optical sections for the boxed regions. The thickness of z-stacks used for maximum projections and/or the single optical sections are 1 µm (optical section) (A), 79.3 and 1 µm (optical section) (B), 39.5 and 0.99 µm (optical section) (C), 52 and 0.4 µm (optical section) (D), 33.7 and 1.4 µm (optical section) (E). Scale bars = 10 µm.

the presence of low concentration (1.3 µg/ml) of CFW (Movie 1). At high concentrations (e.g., 1 mg/ml), pollen tubes burst or stopped growing when the dye was injected in the IBIDI channels containing suspension of growing pollen tubes. Movie 1 acquired using 1.3 µg/ml of CFW illustrates that the signal at the tip of the pollen tube is dim and increases towards distal regions (see also Fig. 7D). In the wake of the progressing tip, the signal increases in the subapical zones. To our knowledge, this is the first time CFW is shown to be useful for live monitoring of cell wall dynamics in pollen tubes. We also noted that, while the signal decreased towards the pollen tube tip, the apical region devoid of signal was considerably shorter than the corresponding pattern observed in fixed samples with the same dye (compare Movie 1 and Fig. 7D with Fig. 5A). Therefore, we suggest that fixation can potentially interfere with binding of some of these probes.

To evaluate the usefulness of COS^{488} for live imaging of pollen tubes, we stained *Camellia*

pollen tubes growing in channels of IBIDI microscope slides. We observed the pollen tubes to continue their growth for several hours after labeling (Movie 2). In Movie 2, signal oscillations can be observed at the tip of the pollen tube, indicating that the signal intensity in fast growing cells needs to be time-resolved through high-frequency image acquisition. Similar to live CFW staining, the decreasing signal gradient towards the tip of the pollen tube was not as dramatic as that in fixed samples (compare Movie 2 and Fig. 7E with Fig. 6A), although it must be noted that the concentration of COS^{488} label in the two experiments were not identical (1:1000 in labeling of fixed and 1:300 in labeling of live samples).

Conclusion

In this technical update, we present simple working protocols for fluorescent labeling of the cell walls of *Arabidopsis* seedlings and *Camellia* pollen tubes using inorganic fluorophores as well as antibodies. We chose the fluorescent labels based on their binding specificity and the availability of published data for validation. Other promising fluorescent probes exist (e.g., Musielak et al., 2015) and should be analyzed for their binding specificity and effect on cell growth in future studies. We discuss different aspects of the labeling results and provide suggestions for tailoring of protocols to different sample types. Cell wall specific antibodies are thought to allow recognizing cell wall polysaccharides with a high degree of specificity. However, their use is not without challenges. Firstly, they are not necessarily always very specific and can bind polysaccharides with similar structures (Hernandez-Gomez et al., 2015). Some of the antibodies available for esterified and demethylesterified pectin, except for cases at the extremities of the esterification spectrum, have overlapping binding ranges (Christiaens et al., 2011, Willats et al., 2000, see Table 2). Further, due to epitope masking (Xue et al., 2013, Marcus et al., 2008) and the relative sizes of the antibody molecules and cell wall pores (e.g., 5-10 nm, Carpita et al., 1979, Berestovsky et al., 2001, McCann et al., 1990) that can limit the penetration of the antibodies (Mravec et al., 2014), fluorescently-tagged antibody molecules may not always be able to access their binding sites resulting in false negatives. Most importantly, antibodies generally require sample fixation prohibiting real-time studying of cell development. We discuss that some cells such as pollen tubes or root hairs can demonstrate strikingly variable cell wall compositions rendering real-time observation a necessity. Fluorescent probes with smaller molecular size and ability to stain samples without fixation, allow the rapid labeling of plant cell structures. However, studies are required to evaluate their binding specificity and their potential to alter the synthesis or assembly of cell wall polysaccharides upon binding, putatively leading to observer's effects (Haigler et al., 1980).

Acknowledgments

This study was supported by a Discovery grant from the Natural Sciences and Engineering Research Council of Canada (NSERC) and by the Canada Research Chair Program. Sample preparation and image acquisition were performed at the McGill University Multi-Scale Imaging Facility, Sainte-Anne-de-Bellevue, Québec, Canada. We thank Dr. Jozef Mravec from the University of Copenhagen for providing us with COS^{488}.

Movie legends

Movie 1. Growing *Camellia japonica* pollen tube stained with 1 µg/ml calcofluor white in liquid medium. The video is composed of maximum projection of z-stacks acquired over 20 time points with 1-min intervals. The right panel shows the bright field channel. The time course experiment was performed using a Zeiss spinning disk microscope (download link).

Movie 2. Growing *Camellia japonica* pollen tube labeled with COS^{488} in liquid medium. The video is composed of maximum projection of z-stacks acquired over 20 time points with 1-min intervals. The time course experiment was performed using a Zeiss LSM 710 confocal microscope (download link).

References

Akkerman, M., Franssen-Verheijen, M., Immerzeel, P., Hollander, L. d., Schel, J. & Emons, A. (2012) Texture of cellulose microfibrils of root hair cell walls of *Arabidopsis thaliana*, *Medicago truncatula*, and *Vicia sativa*. *J. Microsc.*, **247,** 60-67.

Altartouri, B. & Geitmann, A. (2015) Understanding plant cell morphogenesis requires real-time monitoring of cell wall polymers. *Curr. Opin. Plant Biol.*, **23,** 76-82.

Amsbury, S., Hunt, L., Elhaddad, N., Baillie, A., Lundgren, M., Verhertbruggen, Y., Scheller, H. V., Knox, J. P., Fleming, A. J. & Gray, J. E. (2016) Stomatal function requires pectin de-methyl-esterification of the guard cell wall. *Curr. Biol.*, **26,** 2899-2906.

Anderson, C. T., Carroll, A., Akhmetova, L. & Somerville, C. (2010) Real-time imaging of cellulose reorientation during cell wall expansion in *Arabidopsis* roots. *Plant Physiol.*, **152,** 787-796.

Anderson, C. T. & Wallace, I. S. (2012) Illuminating the wall: using click chemistry to image pectins in *Arabidopsis* cell walls. *Plant Signal. Behav.*, **7,** 661-663.

Aouar, L., Chebli, Y. & Geitmann, A. (2010) Morphogenesis of complex plant cell shapes: the mechanical role of crystalline cellulose in growing pollen tubes. *Sex Plant Reprod.*, **23,** 15-27.

Aylor, D. E., Parlange, J. Y. & Krikorian, A. D. (1973) Stomatal mechanics. *Am. J. Bot.*, **60,** 163-171.

Baskin, T. I. (2005) Anisotropic expansion of the plant cell wall. *Annu. Rev. Cell Dev. Biol.*, **21,** 203-222.

Bedrick, A. E. (1968) Rapid one-solution differential staining with textile dyes: Pontacyl dark green B and Pontamine Fast Scarlet 4BA. *Stain Technol.*, **43,** 321-325.

Berestovsky, G. N., Ternovsky, V. I. & Kataev, A. A. (2001) Through pore diameter in the cell wall of Chara corallina. *J. Exp. Bot.*, **52,** 1173-1177.

Biagini, G., Faleri, C., Cresti, M. & Cai, G. (2014) Sucrose concentration in the growth medium affects the cell wall composition of tobacco pollen tubes. *Plant Reprod.*, **27,** 129-144.

Bidhendi, A. J., Altartouri, B., Gosselin, F. P. & Geitmann, A. (2019) Mechanical stress initiates and sustains the morphogenesis of wavy leaf epidermal cells. *Cell Rep.*, **28,** 1237-1250.

Bidhendi, A. J. & Geitmann, A. (2016) Relating the mechanics of the primary plant cell wall to morphogenesis. *J. Exp. Bot.*, **67,** 449-461.

Bidhendi, A. J. & Geitmann, A. (2018) Finite element modeling of shape changes in plant cells. *Plant Physiol.*, **176,** 41-56.

Bidhendi, A. J. & Geitmann, A. (2019a) Geometrical details matter for mechanical modeling of cell morphogenesis. *Dev. Cell*, **50,** 117-125. e112.

Bidhendi, A. J. & Geitmann, A. (2019b) Methods to quantify primary plant cell wall mechanics. *J. Exp. Bot.*, **70,** 3615-3648.

Blake, A. W., McCartney, L., Flint, J. E., Bolam, D. N., Boraston, A. B., Gilbert, H. J. & Knox, J. P. (2006) Understanding the biological rationale for the diversity of cellulose-directed carbohydrate-binding modules in prokaryotic enzymes. *J. Biol. Chem.*, **281,** 29321-29329.

Burgert, I. & Fratzl, P. (2009) Plants control the properties and actuation of their organs through the orientation of cellulose fibrils in their cell walls. *Integr. Comp. Biol.*, **49,** 69-79.

Burn, J. E., Hocart, C. H., Birch, R. J., Cork, A. C. & Williamson, R. E. (2002) Functional analysis of the cellulose cynthase genes *CesA1*, *CesA2*, and *CesA3* in *Arabidopsis*. *Plant Physiol.*, **129,** 797-807.

Carol, R. J. & Dolan, L. (2002) Building a hair: tip growth in *Arabidopsis thaliana* root hairs. *Philos. Trans. R. Soc. Lond. B Biol. Sci.*, **357,** 815-821.

Carpita, N., Sabularse, D., Montezinos, D. & Delmer, D. P. (1979) Determination of the pore size of cell walls of living plant cells. *Science*, **205,** 1144-1147.

Carter, R., Woolfenden, H., Baillie, A., Amsbury, S., Carroll, S., Healicon, E., Sovatzoglou, S., Braybrook, S., Gray, J. E. & Hobbs, J. (2017) Stomatal opening involves polar, not radial, stiffening of guard cells. *Curr. Biol.*, **27,** 2974-2983. e2972.

Chebli, Y. & Geitmann, A. (2007) Mechanical principles governing pollen tube growth. *Funct. Plant Sci. Biotechnol.*, **1,** 232-245.

Chebli, Y. & Geitmann, A. (2015) Live cell and immuno-labeling techniques to study gravitational effects on

single plant cells. In: *Plant Gravitropism*, 209-226. Humana Press, New York, NY.

Chebli, Y., Kaneda, M., Zerzour, R. & Geitmann, A. (2012) The cell wall of the *Arabidopsis* pollen tube—spatial distribution, recycling, and network formation of polysaccharides. *Plant Physiol.*, **160,** 1940-1955.

Chebli, Y., Pujol, L., Shojaeifard, A., Brouwer, I., van Loon, J. J. & Geitmann, A. (2013) Cell wall assembly and intracellular trafficking in plant cells are directly affected by changes in the magnitude of gravitational acceleration. *PLoS One*, **8,** e58246.

Chen, T., Wu, X., Chen, Y., Li, X., Huang, M., Zheng, M., Baluška, F., Šamaj, J. & Lin, J. (2009) Combined proteomic and cytological analysis of Ca^{2+}-calmodulin regulation in *Picea meyeri* pollen tube growth. *Plant Physiol.*, **149,** 1111-1126.

Christiaens, S., Van Buggenhout, S., Ngouémazong, E. D., Vandevenne, E., Fraeye, I., Duvetter, T., Van Loey, A. M. & Hendrickx, M. E. (2011) Anti-homogalacturonan antibodies: A way to explore the effect of processing on pectin in fruits and vegetables? *Food Res. Int.*, **44,** 225-234.

Cook, G. (1940) A lecture experiment on dyeing. *J. Chem. Educ.*, **17,** 330.

Cooke, J. R., De Baerdemaeker, J. G., Rand, R. H. & Mang, H. A. (1976) A finite element shell analysis of guard cell deformations. *Trans. ASAE*, **19,** 1107-1121.

Cornuault, V., Buffetto, F., Rydahl, M. G., Marcus, S. E., Torode, T. A., Xue, J., Crépeau, M.-J., Faria-Blanc, N., Willats, W. G. & Dupree, P. (2015) Monoclonal antibodies indicate low-abundance links between heteroxylan and other glycans of plant cell walls. *Planta*, **242,** 1321-1334.

Cosgrove, D. J. (2014) Re-constructing our models of cellulose and primary cell wall assembly. *Curr. Opin. Plant Biol.*, **22,** 122-131.

Cosgrove, D. J. (2015) Plant cell wall extensibility: connecting plant cell growth with cell wall structure, mechanics, and the action of wall-modifying enzymes. *J. Exp. Bot.*, **67,** 463-476.

Cosgrove, D. J. (2018) Diffuse growth of plant cell walls. *Plant Physiol.*, **176,** 16-27.

Dardelle, F., Lehner, A., Ramdani, Y., Bardor, M., Lerouge, P., Driouich, A. & Mollet, J.-C. (2010) Biochemical and immunocytological characterizations of *Arabidopsis* pollen tube cell wall. *Plant Physiol.*, **153,** 1563-1576.

De Storme, N. & Geelen, D. (2014) Callose homeostasis at plasmodesmata: molecular regulators and developmental relevance. *Front. Plant Sci.*, **5,** 138.

Drakakaki, G. (2015) Polysaccharide deposition during cytokinesis: challenges and future perspectives. *Plant Sci.*, **236,** 177-184.

Echevin, E., Le Gloanec, C., Skowrońska, N., Routier-Kierzkowska, A.-L., Burian, A. & Kierzkowski, D. (2019) Growth and biomechanics of shoot organs. *J. Exp. Bot.*, **70,** 3573-3585.

Fabrice, T. N., Vogler, H., Draeger, C., Munglani, G., Gupta, S., Herger, A. G., Knox, P., Grossniklaus, U. & Ringli, C. (2018) LRX proteins play a crucial role in pollen grain and pollen tube cell wall development. *Plant Physiol.*, **176,** 1981-1992.

Fayant, P., Girlanda, O., Chebli, Y., Aubin, C.-É., Villemure, I. & Geitmann, A. (2010) Finite element model of polar growth in pollen tubes. *Plant Cell*, **22,** 2579-2593.

Ferguson, C., Teeri, T., Siika-aho, M., Read, S. & Bacic, A. (1998) Location of cellulose and callose in pollen tubes and grains of *Nicotiana tabacum*. *Planta*, **206,** 452-460.

Flores-Félix, J. D., Menéndez, E., Marcos-García, M., Celador-Lera, L. & Rivas, R. (2015) Calcofluor white, an alternative to propidium iodide for plant tissues staining in studies of root colonization by fluorescent-tagged rhizobia. *J. Adv. Biol. Biotechnol.***,** 65-70.

Follain, G., Mercier, L., Osmani, N., Harlepp, S. & Goetz, J. G. (2017) Seeing is believing–multi-scale spatio-temporal imaging towards in vivo cell biology. *J. Cell Sci.*, **130,** 23-38.

Fujita, M., Himmelspach, R., Ward, J., Whittington, A., Hasenbein, N., Liu, C., Truong, T. T., Galway, M. E., Mansfield, S. D. & Hocart, C. H. (2013) The *anisotropy1* D604N mutation in the *Arabidopsis* Cellulose Synthase1 catalytic domain reduces cell wall crystallinity and the velocity of cellulose synthase complexes. *Plant Physiol.*, **162,** 74-85.

Galatis, B. & Mitrakos, K. (1980) The ultrastructural cytology of the differentiating guard cells of *Vigna sinensis*. *Am. J. Bot.*, **67,** 1243-1261.

Geitmann, A. (2010a) How to shape a cylinder: pollen tube as a model system for the generation of complex cellular geometry. *Sex Plant Reprod.*, **23,** 63-71.

Geitmann, A. (2010b) Mechanical modeling and structural analysis of the primary plant cell wall. *Curr. Opin. Plant Biol.*, **13,** 693-699.

Geitmann, A. & Dumais, J. (2009) Not-so-tip-growth. *Plant Signal. Behav.*, **4,** 136-138.

Gu, F., Bringmann, M., Combs, J. R., Yang, J., Bergmann, D. C. & Nielsen, E. (2016) *Arabidopsis* CSLD5 functions in cell plate formation in a cell cycle-dependent manner. *Plant Cell*, **28,** 1722-1737.

Haigler, C. H., Brown, R. M. & Benziman, M. (1980) Calcofluor white ST alters the in vivo assembly of cellulose microfibrils. *Science*, **210,** 903-906.

Hall, M., Bansal, P., Lee, J. H., Realff, M. J. & Bommarius, A. S. (2010) Cellulose crystallinity–a key predictor of the enzymatic hydrolysis rate. *FEBS J*, **277,** 1571-1582.

Hasegawa, Y., Nakamura, S., Uheda, E. & Nakamura, N. (2000) Immunolocalization and possible roles of pectins during pollen growth and callose plug formation in angiosperms. *Grana*, **39,** 46-55.

Hernandez-Gomez, M. C., Rydahl, M. G., Rogowski, A., Morland, C., Cartmell, A., Crouch, L., Labourel, A., Fontes, C. M., Willats, W. G. & Gilbert, H. J. (2015)

Recognition of xyloglucan by the crystalline cellulose-binding site of a family 3a carbohydrate-binding module. *FEBS Lett.*, **589,** 2297-2303.

Herth, W. & Schnepf, E. (1980) The fluorochrome, calcofluor white, binds oriented to structural polysaccharide fibrils. *Protoplasma*, **105,** 129-133.

Hervé, C., Marcus, S. E. & Knox, J. P. (2011) Monoclonal antibodies, carbohydrate-binding modules, and the detection of polysaccharides in plant cell walls. In: *The plant cell wall*, 103-113. Springer.

Huff, J., Bergter, A., Birkenbeil, J., Kleppe, I., Engelmann, R. & Krzic, U. (2017) The new 2D Superresolution mode for ZEISS Airyscan. *Nat. Methods*, **14,** 1223.

Hughes, J. & McCully, M. E. (1975) The use of an optical brightener in the study of plant structure. *Stain Technol.*, **50,** 319-329.

Inada, S., Tominaga, M. & Shimmen, T. (2000) Regulation of root growth by gibberellin in *Lemna minor*. *Plant Cell Physiol.*, **41,** 657-665.

Kaplan, J. L., Torode, T. A., Daher, F. B. & Braybrook, S. A. (2019) On pectin methyl-esterification: Implications for in vitro and In vivo viscoelasticity. *BioRxiv***,** 565614, doi.org/565610.561101/565614.

Knox, J. (1992) Molecular probes for the plant cell surface. *Protoplasma*, **167,** 1-9.

Knox, J. P., Linstead, P. J., King, J., Cooper, C. & Roberts, K. (1990) Pectin esterification is spatially regulated both within cell walls and between developing tissues of root apices. *Planta*, **181,** 512-521.

Lampugnani, E. R., Moller, I. E., Cassin, A., Jones, D. F., Koh, P. L., Ratnayake, S., Beahan, C. T., Wilson, S. M., Bacic, A. & Newbigin, E. (2013) In vitro grown pollen tubes of *Nicotiana alata* actively synthesise a fucosylated xyloglucan. *PLoS One*, **8,** e77140.

Leszczuk, A., Kozioł, A., Szczuka, E. & Zdunek, A. (2019) Analysis of AGP contribution to the dynamic assembly and mechanical properties of cell wall during pollen tube growth. *Plant Sci.*, **281,** 9-18.

Levesque-Tremblay, G., Pelloux, J., Braybrook, S. A. & Müller, K. (2015) Tuning of pectin methylesterification: consequences for cell wall biomechanics and development. *Planta*, **242,** 791-811.

Liesche, J., Ziomkiewicz, I. & Schulz, A. (2013) Super-resolution imaging with Pontamine Fast Scarlet 4BS enables direct visualization of cellulose orientation and cell connection architecture in onion epidermis cells. *BMC Plant Biol.*, **13,** 226.

Liners, F., Letesson, J.-J., Didembourg, C. & Van Cutsem, P. (1989) Monoclonal antibodies against pectin: recognition of a conformation induced by calcium. *Plant Physiol.*, **91,** 1419-1424.

Liners, F. & Van Cutsem, P. (1992) Distribution of pectic polysaccharides throughout walls of suspension-cultured carrot cells. *Protoplasma*, **170,** 10-21.

Lundgren, M. R. & Fleming, A. J. (2019) Cellular perspectives for improving mesophyll conductance. *Plant J.*, **101,** 845-857.

Maeda, H. & Ishida, N. (1967) Specificity of binding of hexopyranosyl polysaccharides with fluorescent brightener. *J. Biochem.*, **62,** 276-278.

Marcus, S. E., Blake, A. W., Benians, T. A., Lee, K. J., Poyser, C., Donaldson, L., Leroux, O., Rogowski, A., Petersen, H. L. & Boraston, A. (2010) Restricted access of proteins to mannan polysaccharides in intact plant cell walls. *Plant J.*, **64,** 191-203.

Marcus, S. E., Verhertbruggen, Y., Hervé, C., Ordaz-Ortiz, J. J., Farkas, V., Pedersen, H. L., Willats, W. G. & Knox, J. P. (2008) Pectic homogalacturonan masks abundant sets of xyloglucan epitopes in plant cell walls. *BMC Plant Biol.*, **8,** 60.

Marković, V., Cvrčková, F., Potocký, M., Pejchar, P., Kollárová, E., Kulich, I., Synek, L. & Žárský, V. (2019) EXO70A2 is critical for the exocyst complex function in *Arabidopsis* pollen. *BioRxiv, doi.org/10.1101/831875***,** 831875.

Mavrakis, M., Pourquié, O. & Lecuit, T. (2010) Lighting up developmental mechanisms: how fluorescence imaging heralded a new era. *Development*, **137,** 373-387.

McCann, M., Wells, B. & Roberts, K. (1990) Direct visualization of cross-links in the primary plant cell wall. *J. Cell Sci.*, **96,** 323-334.

McCartney, L., Marcus, S. E. & Knox, J. P. (2005) Monoclonal antibodies to plant cell wall xylans and arabinoxylans. *J. Histochem. Cytochem.*, **53,** 543-546.

Mendrinna, A. & Persson, S. (2015) Root hair growth: it's a one way street. *F1000prime Rep.*, **7,** 23.

Moreno, N., Bougourd, S., Haseloff, J. & Feijó, J. A. (2006) Imaging plant cells. In: *Handbook of biological confocal microscopy*, 769-787. Springer, Boston, MA.

Mravec, J., Kračun, S. K., Rydahl, M. G., Westereng, B., Miart, F., Clausen, M. H., Fangel, J. U., Daugaard, M., Van Cutsem, P. & Henrik, H. (2014) Tracking developmentally regulated post-synthetic processing of homogalacturonan and chitin using reciprocal oligosaccharide probes. *Development*, **141,** 4841-4850.

Mravec, J., Kračun, S. K., Rydahl, M. G., Westereng, B., Pontiggia, D., De Lorenzo, G., Domozych, D. S. & Willats, W. G. (2017) An oligogalacturonide-derived molecular probe demonstrates the dynamics of calcium-mediated pectin complexation in cell walls of tip-growing structures. *Plant J.*, **91,** 534-546.

Murashige, T. & Skoog, F. (1962) A revised medium for rapid growth and bio assays with tobacco tissue cultures. *Physiol. Plant.*, **15,** 473-497.

Musielak, T. J., Schenkel, L., Kolb, M., Henschen, A. & Bayer, M. (2015) A simple and versatile cell wall staining protocol to study plant reproduction. *Plant Reprod.*, **28,** 161-169.

Newcomb, E. H. & Bonnett, H. T. (1965) Cytoplasmic microtubule and wall microfibril orientation in root hairs of radish. *J. Cell Biol.,* **27,** 575-589.

Novy, V., Aïssa, K., Nielsen, F., Straus, S. K., Ciesielski, P., Hunt, C. G. & Saddler, J. (2019) Quantifying cellulose accessibility during enzyme-mediated deconstruction using 2 fluorescence-tagged carbohydrate-binding modules. *Proc. Natl. Acad. Sci. USA,* **116,** 22545-22551.

Paës, G. (2014) Fluorescent probes for exploring plant cell wall deconstruction: a review. *Molecules,* **19,** 9380-9402.

Palevitz, B. & Hepler, P. (1976) Cellulose microfibril orientation and cell shaping in developing guard cells of Allium: the role of microtubules and ion accumulation. *Planta,* **132,** 71-93.

Panteris, E. & Galatis, B. (2005) The morphogenesis of lobed plant cells in the mesophyll and epidermis: organization and distinct roles of cortical microtubules and actin filaments. *New Phytol.,* **167,** 721-732.

Park, S., Szumlanski, A. L., Gu, F., Guo, F. & Nielsen, E. (2011) A role for CSLD3 during cell-wall synthesis in apical plasma membranes of tip-growing root-hair cells. *Nat. Cell Biol.,* **13,** 973.

Parre, E. & Geitmann, A. (2005) Pectin and the role of the physical properties of the cell wall in pollen tube growth of *Solanum chacoense*. *Planta,* **220,** 582-592.

Parrotta, L., Faleri, C., Guerriero, G. & Cai, G. (2019) Cold stress affects cell wall deposition and growth pattern in tobacco pollen tubes. *Plant Sci.,* **283,** 329-342.

Pattathil, S., Avci, U., Baldwin, D., Swennes, A. G., McGill, J. A., Popper, Z., Bootten, T., Albert, A., Davis, R. H. & Chennareddy, C. (2010) A comprehensive toolkit of plant cell wall glycan-directed monoclonal antibodies. *Plant Physiol.,* **153,** 514-525.

Puhlmann, J., Bucheli, E., Swain, M. J., Dunning, N., Albersheim, P., Darvill, A. G. & Hahn, M. G. (1994) Generation of monoclonal antibodies against plant cell-wall polysaccharides. I. Characterization of a monoclonal antibody to a terminal alpha-(1-->2)-linked fucosyl-containing epitope. *Plant Physiol.,* **104,** 699-710.

Roca-Cusachs, P., Conte, V. & Trepat, X. (2017) Quantifying forces in cell biology. *Nat. Cell Biol.,* **19,** 742-751.

Röckel, N., Wolf, S., Kost, B., Rausch, T. & Greiner, S. (2008) Elaborate spatial patterning of cell-wall PME and PMEI at the pollen tube tip involves PMEI endocytosis, and reflects the distribution of esterified and de-esterified pectins. *Plant J.,* **53,** 133-143.

Rongpipi, S., Ye, D., Gomez, E. D. & Gomez, E. W. (2019) Progress and opportunities in the characterization of cellulose–an important regulator of cell wall growth and mechanics. *Front. Plant Sci.,* **9,** 1894.

Rounds, C. M. & Bezanilla, M. (2013) Growth mechanisms in tip-growing plant cells. *Annu. Rev. Plant Biol.,* **64,** 243-265.

Rounds, C. M., Lubeck, E., Hepler, P. K. & Winship, L. J. (2011) Propidium iodide competes with Ca^{2+} to label pectin in pollen tubes and *Arabidopsis* root hairs. *Plant Physiol.,* **157,** 175-187.

Rui, Y., Chen, Y., Kandemir, B., Yi, H., Wang, J. Z., Puri, V. M. & Anderson, C. T. (2018) Balancing strength and flexibility: how the synthesis, organization, and modification of guard cell walls govern stomatal development and dynamics. *Front. Plant Sci.,* **9,** 1202.

Rui, Y., Chen, Y., Yi, H., Purzycki, T., Puri, V. M. & Anderson, C. T. (2019) Synergistic pectin degradation and guard cell pressurization underlie stomatal pore formation. *Plant Physiol.,* **180,** 66-77.

Ruprecht, C., Bartetzko, M. P., Senf, D., Dallabernadina, P., Boos, I., Andersen, M. C., Kotake, T., Knox, J. P., Hahn, M. G. & Clausen, M. H. (2017) A synthetic glycan microarray enables epitope mapping of plant cell wall glycan-directed antibodies. *Plant Physiol.,* **175,** 1094-1104.

Rydahl, M. G., Hansen, A. R., Kračun, S. K. & Mravec, J. (2018) Report on the current inventory of the toolbox for plant cell wall analysis: proteinaceous and small molecular probes. *Front. Plant Sci.,* **9,** 581.

Sahl, S. J., Hell, S. W. & Jakobs, S. (2017) Fluorescence nanoscopy in cell biology. *Nat. Rev. Mol. Cell Biol.,* **18,** 685.

Samaj, J., Komis, G., Novak, D., Ovecka, M. & Samajova, O. (2017) Advances in imaging plant cell dynamics. *Plant Physiol.,* **176,** 80-93.

Schermelleh, L., Ferrand, A., Huser, T., Eggeling, C., Sauer, M., Biehlmaier, O. & Drummen, G. P. (2019) Super-resolution microscopy demystified. *Nat. Cell Biol.,* **21,** 72-84.

Schindelin, J., Arganda-Carreras, I., Frise, E., Kaynig, V., Longair, M., Pietzsch, T., Preibisch, S., Rueden, C., Saalfeld, S. & Schmid, B. (2012) Fiji: an open-source platform for biological-image analysis. *Nat. Methods,* **9,** 676.

Sede, A. R., Borassi, C., Wengier, D. L., Mecchia, M. A., Estevez, J. M. & Muschietti, J. P. (2018) *Arabidopsis* pollen extensins LRX are required for cell wall integrity during pollen tube growth. *FEBS letters,* **592,** 233-243.

Somerville, C., Bauer, S., Brininstool, G., Facette, M., Hamann, T., Milne, J., Osborne, E., Paredez, A., Persson, S. & Raab, T. (2004) Toward a systems approach to understanding plant cell walls. *Science,* **306,** 2206-2211.

Specht, E. A., Braselmann, E. & Palmer, A. E. (2017) A critical and comparative review of fluorescent tools for live-cell imaging. *Annu. Rev. Physiol.,* **79,** 93-117.

Verhertbruggen, Y., Marcus, S. E., Haeger, A., Ordaz-Ortiz, J. J. & Knox, J. P. (2009) An extended set of monoclonal antibodies to pectic homogalacturonan. *Carbohydr. Res.,* **344,** 1858-1862.

Vőfély, R. V., Gallagher, J., Pisano, G. D., Bartlett, M. & Braybrook, S. A. (2019) Of puzzles and pavements: a

quantitative exploration of leaf epidermal cell shape. *New Phytol.*, **221,** 540-552.

Voiniciuc, C., Pauly, M. & Usadel, B. (2018) Monitoring polysaccharide dynamics in the plant cell wall. *Plant Physiol.*, **176,** 2590-2600.

Wallace, I. & Anderson, C. T. (2012) Small molecule probes for plant cell wall polysaccharide imaging. *Front. Plant Sci.*, **3,** 89.

Wang, H., Zhuang, X., Cai, Y., Cheung, A. Y. & Jiang, L. (2013) Apical F-actin-regulated exocytic targeting of NtPPME1 is essential for construction and rigidity of the pollen tube cell wall. *Plant J.*, **76,** 367-379.

Willats, W. G., Limberg, G., Buchholt, H. C., van Alebeek, G.-J., Benen, J., Christensen, T. M., Visser, J., Voragen, A., Mikkelsen, J. D. & Knox, J. P. (2000) Analysis of pectic epitopes recognised by hybridoma and phage display monoclonal antibodies using defined oligosaccharides, polysaccharides, and enzymatic degradation. *Carbohydr. Res.*, **327,** 309-320.

Xue, J., Bosch, M. & Knox, J. P. (2013) Heterogeneity and glycan masking of cell wall microstructures in the stems of *Miscanthus x giganteus*, and its parents *M. sinensis* and *M. sacchariflorus*. *PLoS One*, **8,** e8211.

Yanagisawa, M., Desyatova, A. S., Belteton, S. A., Mallery, E. L., Turner, J. A. & Szymanski, D. B. (2015) Patterning mechanisms of cytoskeletal and cell wall systems during leaf trichome morphogenesis. *Nat. Plant*, **1,** 15014.

Yi, H., Rui, Y., Kandemir, B., Wang, J. Z., Anderson, C. T. & Puri, V. M. (2018) Mechanical effects of cellulose, xyloglucan, and pectins on stomatal guard cells of *Arabidopsis thaliana*. *Front. Plant Sci.*, **9,** 1566.

Zamil, M. & Geitmann, A. (2017) The middle lamella—more than a glue. *Phys. Biol.*, **14,** 015004.

Zanella, R., Zanghirati, G., Cavicchioli, R., Zanni, L., Boccacci, P., Bertero, M. & Vicidomini, G. (2013) Towards real-time image deconvolution: application to confocal and STED microscopy. *Sci. Rep.*, **3,** 2523.

Zhang, M., Zhang, R., Qu, X. & Huang, S. (2016) *Arabidopsis* FIM5 decorates apical actin filaments and regulates their organization in the pollen tube. *J. Exp. Bot.*, **67,** 3407-3417.

Zhang, T., Tang, H., Vavylonis, D. & Cosgrove, D. J. (2019) Disentangling loosening from softening: insights into primary cell wall structure. *Plant J.*, **100,** 1101-1117.

Zhao, Y., Man, Y., Wen, J., Guo, Y. & Lin, J. (2019) Advances in imaging plant cell walls. *Trends Plant Sci.*, **24,** 867-878.